Design and Analysis of Active Aerodynamic Control Systems for Increasing the Safety of High-Speed Road Vehicles

by

Mohammed Hammad

A thesis submitted to the
School of Graduate and Postdoctoral Studies in partial
fulfillment of the requirements for the degree of

Master of Applied Science in Automotive Engineering

Faculty of Engineering and Applied Science
University of Ontario Institute of Technology
Oshawa, Ontario, Canada

July 2019

THESIS EXAMINATION INFORMATION

Submitted by: **Mohammed Hammad**

Master of Applied Science in **Automotive Engineering**

Thesis title: Design and Analysis of Active Aerodynamic Control Systems for Increasing the Safety of High-Speed Road Vehicles

An oral defense of this thesis took place on July 23, 2019 in front of the following examining committee:

Examining Committee:

Chair of Examining Committee	Dr. Jing Ren
Research Supervisor	Dr. Yuping He
Examining Committee Member	Dr. Martin Agelin-Chaab
External Examiner	Dr. Mohamed Youssef

The above committee determined that the thesis is acceptable in form and content and that a satisfactory knowledge of the field covered by the thesis was demonstrated by the candidate during an oral examination. A signed copy of the Certificate of Approval is available from the School of Graduate and Postdoctoral Studies.

Abstract

The lateral stability and the safety of road vehicles is dependent on the vehicle design and operating conditions. Under operating conditions such as slippery roads, high lateral acceleration and tight cornering, the forces and torques due to the interactions between the tire and road may be saturated. Various active safety systems have been proposed and developed to mitigate these concerns but they all work based on the manipulation of tire forces. Thus, the capability of the current active safety systems cannot go beyond the performance limitation determined by the interactions between the tire and road. On the other hand, at high speeds, significant downforce can be generated by employing aerodynamic wings on the vehicle body to enhance its road holding ability. A split rear wing is proposed to control the aerodynamics of high-speed road vehicles to closely manipulate the dynamics of the vehicle. A nonlinear vehicle model is derived to simulate the vehicle's lateral dynamics and an airfoil with a high lift to drag ratio is used to design the rear wing. A sliding mode control technique is used to design the active aerodynamic controller to achieve the objective of tracking the desired steady-state yaw rate. The selection of the control technique and the control objective is shown to be comprehensive and satisfactorily improve the handling performance. The controller design is validated using co-simulation implemented in the combined CarSim-MATLAB/Simulink simulation environment. Simulation results demonstrate that active aerodynamic control improves the lateral stability of the vehicle and that the improvement is more pronounced as the vehicle forward speed increases. The enhancement in lateral performance and road holding capability is also presented.

Keywords: road vehicles; lateral stability; active safety systems; aerodynamic control; sliding mode control; split rear wing.

Authors Declaration

I hereby declare that this thesis consists of original work of which I have authored. This is a true copy of the thesis, including any required final revisions, as accepted by my examiners.

I authorize the University of Ontario Institute of Technology to lend this thesis to other institutions or individuals for the purpose of scholarly research. I further authorize University of Ontario Institute of Technology to reproduce this thesis by photocopying or by other means, in total or in part, at the request of other institutions or individuals for the purpose of scholarly research. I understand that my thesis will be made electronically available to the public.

Mohammed Hammad

Statement of Contributions

Part of this work has been published in conferences as:

1. Hammad, M., Qureshi, K., and He, Y.. Safety and Lateral Dynamics Improvement of a Race Car Using Active Rear Wing Control. No. 2019-01-0643. SAE Technical Paper, 2019.

2. Hammad, M. and He, Y.. A Review of Active Aerodynamic Control for Increasing Safety of High-Speed Road Vehicles. CSME International Congress, 2019. (In Press)

Acknowledgement

First and foremost, praise and thanks be to Allah with the blessings and mercy of whom I have been able to complete this enthralling journey.

I am very grateful to my supervisor, Dr. Yuping He, for giving me the opportunity to join his research lab and pursue MASc and for following that up with his endless support and motivation. I found a fitting environment in his lab to thrive. He understood and supported me on multiple occasions with my personal situations. Last but not the least, he helped me pursue my academic interests by supporting me for different conferences.

My father, Mohammed Ismail, exhibited immense patience and unconditionally supported me while enduring hardship himself; I feel privileged to be his son. I am also deeply thankful to my sister, Samiah, and my two brothers, Ammar and Hassan, for their constant encouragement and for understanding my work.

Finally, I would like to thank my friends without whom this journey would not have been possible. Mutaz, Priya, Khizar and Abhilash for being there with me in the ups and downs and for pulling and pushing me to this point, Farhan for his timely words of wisdom, Daniyal for making me feel at home while I am miles away from my actual one, Talha Zia and Sohail Patel for being brotherly figures, Tariq and Fahad for being supportive housemates and Salman for always showing belief in me.

To my parents, Mohammed Ismail and Farzana Naseem.

Table of Contents

List of Tables

List of Figures

List of Abbreviations and Symbols

Abbreviations

AAD	Active aerodynamic(s)
ASS	Active safety system(s)
CFD	Computational fluid dynamics
CG	Center of gravity of the vehicle
DOF	Degrees of Freedom
SMC	Sliding mode control

Notations

a	Perpendicular distance of the CG of the wings from the centreline of the vehicle
A_{dr}	Reference area for drag coefficient calculation
A_{dw}	Reference area for downforce coefficient calculation
b	Perpendicular distance of the CG of the wings from the CG of the vehicle
C	Damping coefficient of the suspension
C_y	Cornering stiffness of the tires
C_{dr}	Drag coefficient
C_{dw}	Downforce coefficient
e	Error function of the SMC
E	Control parameter of the SMC
g	Acceleration due to gravity

h	Height of the CG of the vehicle from the ground
h_{roll}	Height of the CG of the vehicle from the roll center
h_f	Height of the CG of front suspension from the ground
h_r	Height of the CG of rear suspension from the ground
h_{12}	Height of the CG of front suspension from the front roll center
h_{34}	Height of the CG of rear suspension from the rear roll center
I_{xx}	Roll inertia of the sprung mass of the vehicle
I_{zz}	Yaw inertia of the sprung mass of the vehicle
F_t	Tractive force generated by a tire
F_s	Side force generated by a tire
F_x	Longitudinal component of the tire forces
F_y	Lateral component of the tire forces
F_z	Normal load on a tire
F_{dr}	Drag force generated by a rear wing
F_{dw}	Downforce generated by a rear wing
K_f	Spring stiffness of the front suspension
K_r	Spring stiffness of the rear suspension
l_1	Distance between CG and the front axle of the vehicle
l_2	Distance between CG and the rear axle of the vehicle
l	Wheelbase; distance between the axles of the vehicle
m_{us}	Unsprung mass of the vehicle of either the front or the rear side
m_s	Sprung mass of the vehicle
m	The total mass of the vehicle
p	The roll rate of the CG of the vehicle

$\dot{p}$	Roll acceleration of the CG of the vehicle
r	Yaw rate of the CG of the vehicle
$\dot{r}$	Yaw rate of the CG of the vehicle
r_{ss}	Steady-state yaw rate
R_s	Ratio of the steering wheel angle to the pinion angle
R_{rp}	Ratio of the rack displacement to the pinion angle
R_{sr}	Ratio of the steering angle to the rack displacement
R_{lsr}	Ratio of the left tire steering to the rack displacement
R_{rsr}	Ratio of the right tire steering to the rack displacement
T	Track width; lateral distance between either the front tires or the rear tires
u	Vehicle's forward velocity
U	Control parameter of the SMC

Greek Letters

α	Slip angle of the tires
β	Sideslip angle of the vehicle
γ	Camber angle of the tires
δ	Tire steering angles
δ_{sw}	Steering wheel angle
κ	Longitudinal slip ratio
μ	Coefficient of friction between the road and the tire
φ	The roll angle of the CG of the vehicle
ψ	Yaw angle of the CG of the vehicle

ρ	Density of air
σ	Sliding surface
θ	The angle of attack of the rear wings

Subscripts

1	Front left
2	Front right
3	Rear left
4	Rear right

For aerodynamic forces, coefficients and reference areas,

1	Left wing
2	Right wing

Chapter 1

Introduction

1.1 Background and Motivation

The movement of a road vehicle is primarily due to the forces generated at the tire-road interface. However, tire forces are limited by the maximum adhesion capability between the tire-road interface. The maximum adhesion capability is a function of the vertical load on the tire and tire-road friction coefficient. Scenarios, such as negotiating around a tight corner at a high speed, traveling on slippery surfaces, etc., may result in losing traction and lateral stability of a vehicle, thereby leading to a large number of road accidents all over the world [1]. Therefore, there is a crucial need to supplement the tire forces to increase the safety of road vehicles and, in particular, those traveling on curved paths at high speeds. Intelligently manipulating the aerodynamics of high-speed road vehicles may meet the critical requirement.

The two main aerodynamic forces are the lift/downside-force and drag. Wings are commonly used in airplanes for the purpose of generating upward forces or lift. Wings may be inverted to create downforces or negative lift. By employing an inverted wing on the rear end of a road vehicle, downside forces can be generated on the vehicle body to increase the road holding capability. On the other hand, the accompanying drag hampers the longitudinal performance of the vehicle in situations which doesn't involve braking. However, as shown in Figure 1.1, a split rear wing can be used to generate a corrective yaw moment by means of setting different attack angles for the right and left wings, thereby improving the yaw stability of the vehicle. This is achieved by the resultant difference between the downforces on the right and left tires [2]. The split allows for the elimination of unnecessary drag forces. Moreover, the split wing can also be used to favorably manipulate the lateral load transfer during cornering maneuvers.

To improve the lateral stability and increase the safety of road vehicles, the proposed split wing should be intelligently controlled and manipulated considering the current vehicle dynamic states, which are determined by the operating conditions, e.g., vehicle forward speed, straight line or curved path, dry or wet road surfaces, etc.

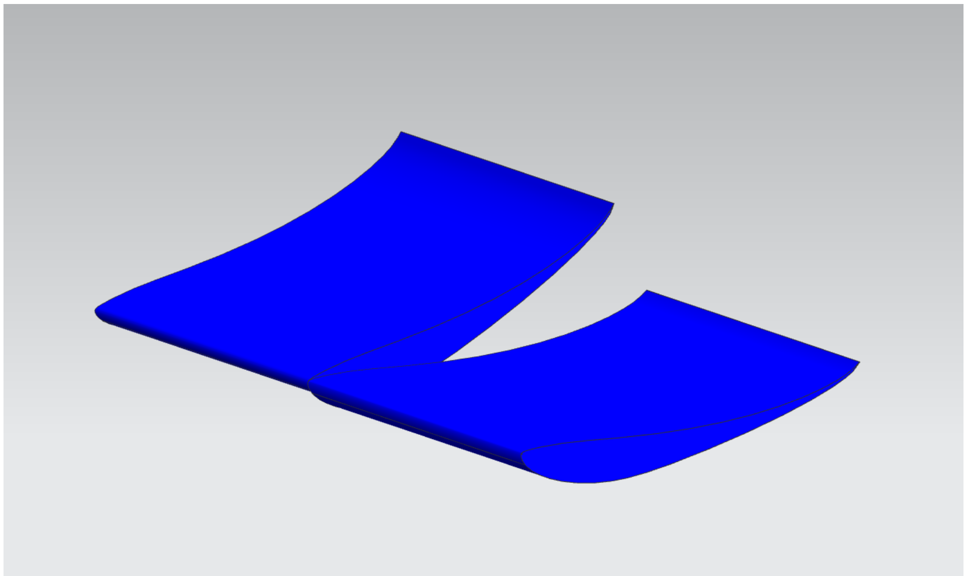

Figure 1.1: A CAD model of a split rear wing with the right and left wings at different attack angles.

Clearly, it is beyond the capability of the driver to control the wings while driving the vehicle by steering and accelerating or braking. Therefore, a control system, namely, the Active Aerodynamic (AAD) System, must be designed to automatically control the attack angles of the two wings. Obviously, intelligent control of the aerodynamic forces can offer additional ways to increase the safety of high-speed road vehicles. In other words, active aerodynamic control can increase the safety of road vehicles by expanding the limited performance. It is indicated that little attention has been paid to the functionality and applicability of the intelligently and adaptively controlled split wings [3, 4]. Hence, there is a compelling need to explore the design methods to fully demonstrate the potential functionality and applicability of the innovative active safety system for high-speed road vehicles.

It is to be noted here that active aerodynamics, in this thesis, is derived from the perspective of vehicle dynamic control which inherently means a control system to operate the movement of aerodynamic surfaces as opposed to the general definition which may involve the operation through manual force.

1.2 Thesis Objectives

- The main objective of this thesis is to design an AAD system, which will increase the safety of high-speed road vehicles.
- To acquire aerodynamic data for the selected wing design using Computational Fluid Dynamics (CFD) simulations which will, in turn, be used for the design of the AAD system.
- To ensure the robust performance of the active aerodynamic control system, which is insensitive to external disturbances, a sliding mode control (SMC) technique is used to design the AAD controller.

- To design, tune and validate the SMC-based AAD controller using three different vehicle models. A linear 2 degrees of freedom (DOF) bicycle model is derived, which is used as a reference model for the design of the SMC-based AAD controller. A nonlinear 3-DOF model is developed, which can be easily combined with the acquired CFD data to simulate the aerodynamic effects on the overall vehicle dynamics. The 3-DOF model will be used to fine-tune the control parameters of the SMC-based AAD controller. To validate the SMC-based AAD controller, a nonlinear 14-DOF model is generated in CarSim software.
- To validate the SMC-based AAD controller using co-simulations in the CarSim-MATLAB/Simulink environment, in which the 14-DOF model developed in CarSim is integrated with the SMC-based AAD controller designed in MATLAB/Simulink using an interface, namely, the S-function.

1.3 Thesis Contributions

- An explicit method is proposed and developed to calculate aerodynamic coefficients, which are used for calculating aerodynamic drag and lift/downside-force. Generally, the aerodynamic coefficients are dependent on projected area of the wing and vehicle forward speed.
- The acquired aerodynamic data is integrated with the derived 3-DOF model and the 14-DOF model developed in CarSim for designing and validating the AAD controller for increasing the safety of high-speed road vehicles.
- An SMC-based AAD controller is proposed and designed, by which the attack angles of the split rear wing are controlled and manipulated to achieve the desired forces and torques to enhance the yaw stability of high-speed road vehicles.

- Co-simulations are conducted in the CarSim-MATLAB/Simulink environment, in which the 14-DOF model developed in CarSim is integrated with the SMC-based AAD controller designed in MATLAB/Simulink using an interface.

1.4 Thesis Organization

The rest of the thesis is organized as follows. Chapter 2 reviews the past studies and gaps in this research topic to be tackled in this thesis. All the relevant and fundamental concepts, principles, and terminologies are also defined and explained in this chapter. Chapter 3 presents the 2-DOF bicycle model, the 3-DOF nonlinear model, and the 14-DOF model developed in CarSim, which are used to design, fine-tune, and validate the proposed AAD controller, respectively. This chapter also presents the chosen wing designed in a CAD environment and the relevant CFD simulations. Chapter 4 introduces the design of the SMC-based AAD controller and evaluates the performance of the SMC-based AAD controller. Chapter 5 validates the proposed AAD controller using the co-simulations. Finally, the conclusions are drawn in Chapter 6.

Chapter 2

Literature Review

2.1 Introduction

Vehicle dynamics control is a process of controlling one or more state variables of a vehicle to improve either one or a combination of performance measures in order to improve the lateral stability and increase the safety. Most of the systems developed to avoid or mitigate the severity of traffic accidents are called active safety systems. To date, various active safety systems have been proposed and developed to increase the safety of road vehicles. These active safety systems include active front/rear steering, torque vectoring, differential braking, active camber control, active roll moment control, active suspension control, etc., [5–9].

Road vehicle aerodynamics concerns the effects arising due to the motion of the vehicle through or relative to the air [10,11]. Aerodynamic drag and lift are two widely used terms for signifying aerodynamic forces in horizontal and vertical directions, respectively. Aerodynamic drag reduction for improving acceleration performance and fuel economy is a well-known research area [12,13]. For high-speed vehicles, efforts to increase negative lift or downforce and thus enhancing the road holding capability of the vehicle are well documented [14]. Some work on identifying and stabilizing the dynamic states of a vehicle under crosswinds is also done, especially on bigger vehicles, e.g., buses and articulated heavy vehicles [15]. Recently, attempts have been made to make mathematical models of the aerodynamic forces and coefficients, accurate and robust to fit into full-scale simulations [16, 17].

Active aerodynamics binds the two relatively distinct fields of ‘vehicle dynamics control’ and ‘aerodynamics of ground vehicles’ as shown in Figure 2.1.

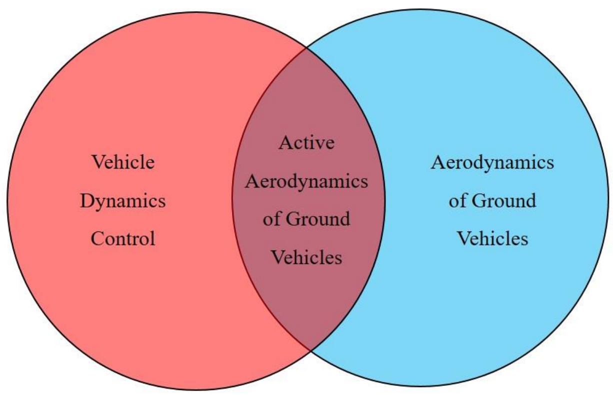

Figure 2.1: Description of active aerodynamics of ground vehicles.

Active aerodynamic control is, thus, to manipulate moving surfaces (bodies) to generate varying aerodynamic forces and moments for enhancing vehicle dynamics and increasing vehicle safety. It is important to note that all the vehicle dynamic control systems developed so far rely on forces generated at the tire-road contact patches and would cease to perform adequately under the saturation of such forces. The saturation limit of these forces is the product of the tire-road coefficient of friction and the vertical load on the tire. Active aerodynamic control systems take into account the forces due to aerodynamics, drag directly and downforce indirectly by increasing the vertical load on tires, for vehicle dynamics control. The effects due to aerodynamics pose impacts on the longitudinal, lateral, and vertical dynamics of road vehicles. Each area of impact will be reviewed in this section.

It is well-known that aerodynamic drag significantly affects the fuel economy and the longitudinal dynamics of road vehicles traveling at high speeds [18]. It is demonstrated that the coefficient of drag of a truck may be reduced by 35% by controlling the boundary layer separation by the momentum injection method using a rotating cylinder. An active flow control method was proposed to reduce the aerodynamic drag of a van [19]. An actively translating rear diffuser device was proposed to reduce the aerodynamic drag experienced by passenger cars [20]. Due to the stringent government standard/regulation requirements on improving the fuel economy and decreasing greenhouse gas emissions, research on active airflow control gains increasing attention.

Active aerodynamic control strategies have also been studied to improve the lateral dynamics of road vehicles, i.e., handling performance and lateral stability. It was shown that aerodynamically generated direct yaw and roll moments can significantly improve the handling and lateral stability of road vehicles [21]. An active aerodynamic system was examined to improve the handling and safety of a small-size race car in a lane-change maneuver and driving on wet roads [22]. Active inverted wings were proposed to increase the downward forces on the tires for enhancing the road holding, thereby improving the handling and stability of race cars [3]. To improve the handling and safety of high-speed vehicles, normal force distribution was controlled by manipulating the angle of attack of the front and rear spoilers, and the performance of the active aerodynamic control system was analyzed through numerical simulation based on a nonlinear vehicle model [4]. A physical prototype of an actively controlled rear wing was fabricated, and the essential design parameters, functionality, and features of the active wing were introduced [23].

Various attempts have been made to enhance vertical vehicle dynamics and improve the ride quality of road vehicles. Doniselli et al. examined the aerodynamic effects on the ride quality of a vehicle running at high speed on randomly profiled roads [24]. Savkoor proposed an aerodynamic control device for reducing pitch and heave of truck cabins [25]. Meijaard et al. investigated the potential for vehicle ride quality improvement using both suspension and aerodynamic actuators [26]. It is shown that combining the active suspension and aerodynamic actuators can achieve a considerable improvement of the ride comfort with a small deterioration of the road holding. Active aerodynamic surfaces were explored to improve vehicle road-holding without affecting ride quality [27]. On the other hand, active aerodynamic surfaces were proposed to improve the ride comfort, and the results showed that the proposed method shows improvements of the order of 30% in ride quality without negative effects on road-holding at high speeds [28]. It is well-known that there is a trade-off between ride quality and road holding capability. The aforementioned studies indicate that active aerodynamic control provides an effective way to relieve the trade-off.

Meanwhile, some studies based only on CFD simulations proved the effectiveness of active aerodynamic control. For the purpose of examining the paradox due to the co-existence of drag and lift of spoilers, CFD simulation was conducted, and the effects of the aerodynamic rear wings' effects on the lateral and longitudinal dynamics were analyzed [2]. To investigate the downforce and drag, as well as their relation, CFD simulations were performed for a car with an active rear split spoiler at different spoiler angle of attack and at different speeds [29]. The simulation results were compared with the experimental data derived from a wind tunnel on the physical car and the spoiler prototype. It is demonstrated that a proposed active split rear wing can improve the lateral stability of a race car over tight cornering maneuver, and will not degrade the longitudinal dynamics of the vehicle [30].

In the following sections, attention will be focused on the following topics: dynamic modeling, aerodynamic forces, and control systems.

2.2 Dynamic Models

Dynamic modeling, here, is referred to the mathematical representation of the forces acting on the vehicle body, including those from the aerodynamic devices and their effect on the vehicle motion. The mathematical representation is often described as a set of ordinary differential equations (ODE's). Dynamic modeling is the first step in the designing of any control system. Generally, with the help of a mathematical representation, state, input, and output variables of the system are clearly defined to develop the control system.

The process to derive the mathematical model starts with the selection of motions to be considered, i.e., the number of degrees of freedom (DOF's).

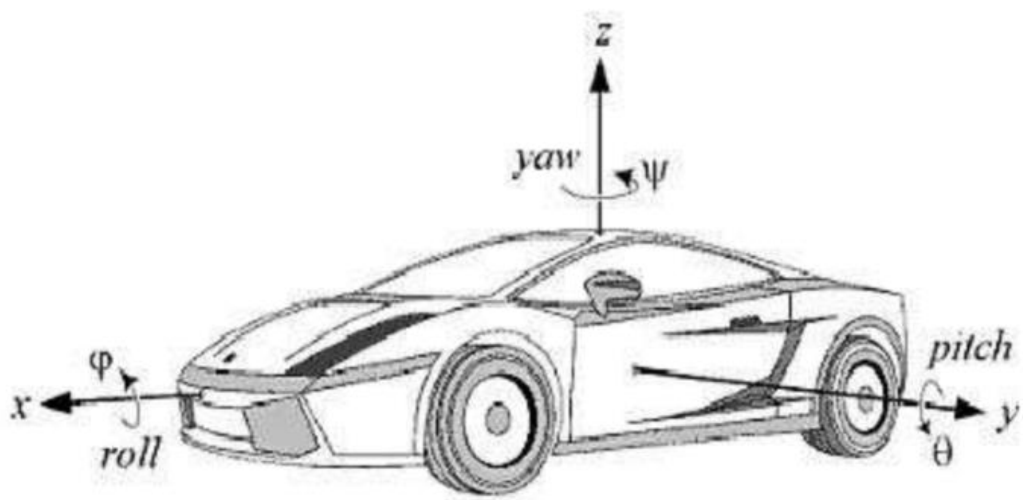

Figure 2.2: Vehicle motion along and about the three principal axes according to ISO standards [32].

A complex version of a vehicle model may include all the six DOF's for the sprung mass and additional DOF's for unsprung masses, e.g., tires and axles. Figure 2.2 describes the six principal motions of the sprung mass in ISO coordinates [31]. A simplified model may only include 3 DOF for sprung mass, considering tire forces as single point forces and neglecting suspension dynamics. The selection is made based on the application of control systems.

Once the number of DOF's are selected, equations of motion for each DOF is derived and these equations of motions are converted to a set of ODE's to demarcate the state and input variables of the system. When examining vehicle handling performance, important states are yaw rate, lateral acceleration, roll angle, roll rate, sideslip angle, etc., [31, 32].

To this end, various vehicle models with different complexity and fidelity have been generated and developed. In addition, to design and develop controllers for active aerodynamic control systems, simplified linear or nonlinear vehicle models have been widely used. It is, hence, very important that an appropriate vehicle model is built or chosen for applications. The equations of a dynamic model must include the aerodynamic forces as inputs to simulate the controlled vehicle. Hence, alongside choosing a dynamic model, selection of the number of wings and their positioning is also an important consideration.

One past research on active aerodynamics for the purpose of improving the handling performance used a 3-DOF model, as shown in Figure 2.3, to analyze vehicle handling under the aerodynamic influence [21].

As shown in Figure 2.4, two different aerodynamic devices were used, which are two rudders (one on the front and the other on the rear of the car) and two rear wings on the rear of the car (not shown in the figure). The two aerodynamic devices construct three different combinations: 1) the front and rear rudders, 2) the two rear wings, and 3) the front rudder and the two rear wings.

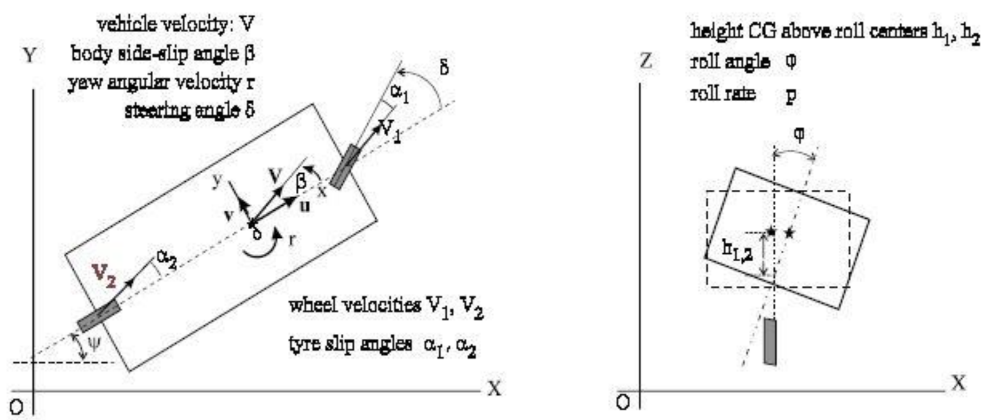

Figure 2.3: A 3-DOF vehicle model [21].

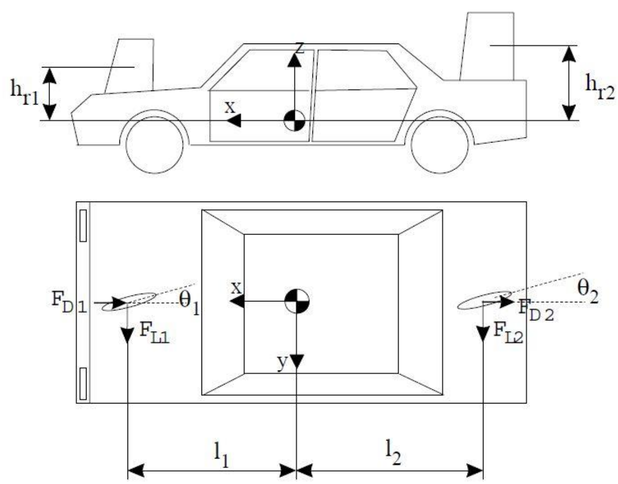

Figure 2.4: Aerodynamic devices (rudders) mounted on a vehicle [21].

The use of rudder devices is questionable due to its mounting location and possible hindrance for both the front and the rear sight of the driver. Additionally, it is hard to imagine the generation of an adequate amount of required corrective moments in the absence of a couple. This configuration could be useful for low-speed ranges, however.

A simple model, neglecting the roll motion, with two rear wings has also been published to design an AAD system [30]. Linear models for estimating handling behavior have the tire forces estimated as a linear function of tire cornering stiffness and slip angle.

However, the application of aerodynamics becomes meaningful at high speeds and tight cornering maneuvers where the vehicle operates beyond the linear dynamic range and exhibits nonlinear dynamic characteristics. Therefore, linear vehicle models cannot simulate the nonlinear dynamic properties and, in particular, the aerodynamic characteristics at high speeds and high lateral accelerations.

To address the shortcomings of linear vehicle models, an 8-DOF nonlinear model with more complexity and high accuracy, as shown in Figure 2.5, was used to study the handling behavior under the action of aerodynamic forces.

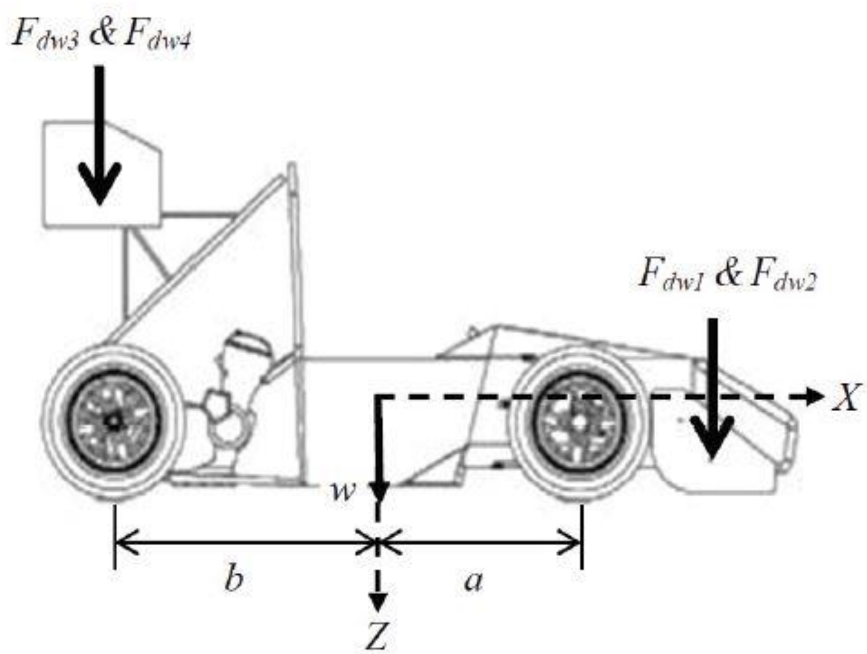

Figure 2.5: An 8-DOF full car model [3].

As shown in Figure 2.6, a 14-DOF model developed in a commercial software package was used to simulate the dynamics of a race car [4].

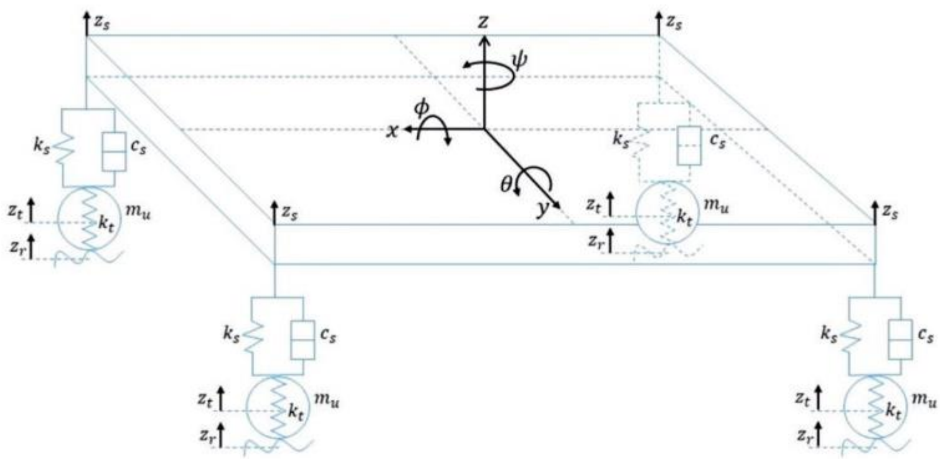

Figure 2.6: A 14-DOF full car model [4].

Built upon the 8-DOF nonlinear model shown in Figure 2.5 [3], the aerodynamic devices used were a 3-element inverted wing for the front axle and a 2-element inverted wing for the rear axle, as shown in Figure 2.7. The aerodynamic devices were used for formula race cars. To incorporate aerodynamic effects into the 14-DOF full car model shown in Figure 2.6, two wings were added, among which one wing was installed on the front end of the car, and the other was equipped on the rear end of the car.

It should be mentioned that the complete full vehicle models (e.g., those shown in Figures 2.5 and 2.6) reported in the literature may achieve high fidelity and accuracy in simulating the dynamics and the effects of aerodynamics [3, 4]. However, these complex vehicle models are not computationally efficient, and not suitable for active aerodynamic controller designs.

Figure 2.7: Aerodynamic devices used for (a) front axle and (b) rear axle [3].

2.3 Aerodynamic Forces

Effective modeling of aerodynamic forces is another necessary step to develop an AAD control system. The aerodynamic drag and lift are commonly determined by the following equations [11]:

$$Drag = \frac{C_D \rho A V^2}{2} \tag{2.1}$$

$$Lift = \frac{C_L \rho A V^2}{2} \tag{2.2}$$

where V denotes vehicle forward speed, A frontal area of the wing, ρ air density, C_D and C_L are aerodynamic drag and lift coefficient, respectively.

It is important to note that the aerodynamic coefficients are not constant but are functions of the projected area of the wing which in turn is dependent on the attack angle of the wing. Aerodynamic data for any given device is either generated from CFD simulations or wind tunnel tests to estimate the aerodynamic coefficients at varying angles of attack. Generally, the aerodynamic data set is fitted into a regular vehicle model to construct a holistic vehicle dynamic model for designing active aerodynamic control systems. Acquiring the aerodynamic data is frequently based on CFD simulations [3, 22], which is expensive in terms of CFD model development, computational efficiency, and analysis cost. In the literature, few investigations have been conducted to examine AAD systems. The other way to acquire aerodynamic data is based on wind tunnel testing [4].

Recently, CFD simulations have been conducted to design optimal wings and configurations, and to determine the optimal positions and orientations of wings [2, 23, 29]. Numerical simulations to simulate the aerodynamic forces and effects on vehicle dynamics have been presented. The achieved results and proposed methods can be considered as an important part in the development of AAD systems for high-speed vehicles.

In this thesis, numerical simulations will be conducted to calculate aerodynamic coefficients at various attack angles and the obtained data will be used in the design of the AAD system.

2.4 Control Systems

To develop an active aerodynamic system for road vehicles, the design objectives and constraints should be specified. The control system design is arguably the crux in the development of an active aerodynamic system. Built upon an established vehicle dynamic model, an AAD controller may be designed using well-established control techniques.

Vehicle dynamics control is a process of achieving the desired state of the vehicle system by manipulating one or more state variables of the system [35]. The set of equations and functions used to execute this process is called a vehicle control system. There are two important components of a vehicle control system design: the control objectives/constraints and the control technique. Control objective could be the stabilization or damping of any of the system's states, forcing any of the states to the desired path, etc. and it depends on the system to be controlled. Control technique is the method of achieving the control objective.

Control systems can be primarily classified into types, i.e., open- and closed-loop control. Open-loop control systems are those, in which the input is independent of the output. For example, an oven that stops running based on a set amount of time is an open-loop control system, that is, the oven stops regardless of the cooking of food. A closed-loop control system, also called feedback control, is that, in which the output of the system is fed back to the system; then the error is calculated and the input signal is varied accordingly to abate the error signal. Modern air conditioners are a good example of a closed-loop control system, in which the sensors check the desired temperature and accordingly, the compressor is switched on or off. Figure 2.8 shows a schematic block diagram of a closed-loop control system.

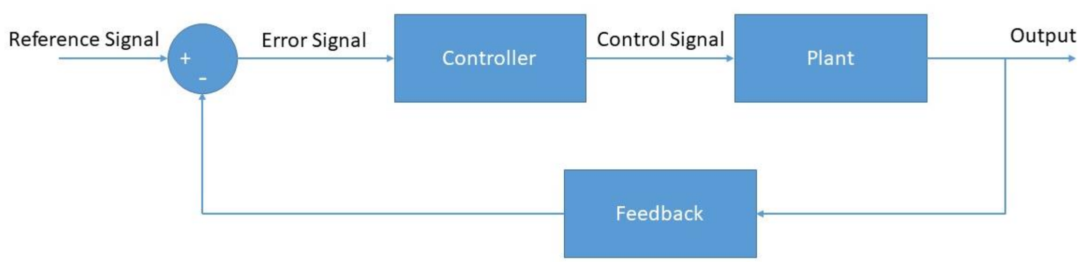

Figure 2.8: Schematic of a closed-loop control system.

Feedback control systems can be further classified according to various control strategies, e.g., optimal control, robust control, adaptive control, intelligent control, stochastic control, etc. Figure 2.9 simply illustrates the classification of feedback control systems. Furthermore, there are a lot of control techniques, e.g., artificial neural networks, genetic algorithms, H-infinity loop shaping, linear quadratic regulator, etc. The control technique(s) may be selected and used in a given control strategy design.

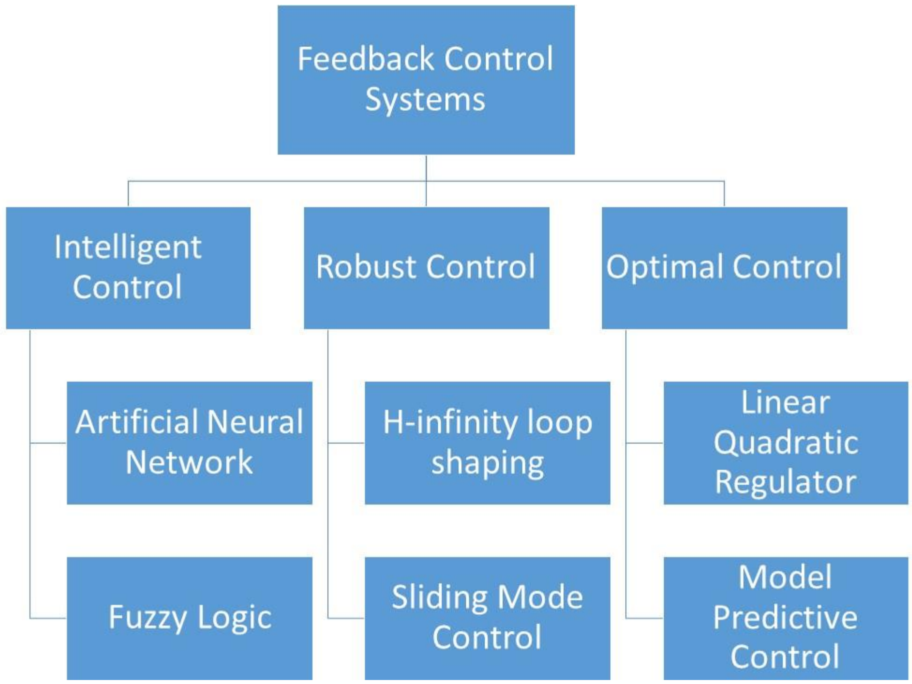

Figure 2.9: Classification of some control systems.

Following the above brief introduction of control systems and its components is a review of the objectives and techniques used in the past for building AAD systems.

Savkoor and Chou proposed two different strategies, namely full state feedback, open-loop feedback with pre-filter, and a combination of both, to calculate the demand on the roll and yaw actuators [21]. Figure 2.10 shows the combined control strategy. This demand would be fulfilled by trying various configurations of rear split spoiler and/or rudder devices at the front and/or rear of the vehicle. The objective of this design was to minimize the body sideslip angle, the roll angle, the roll rate, and to track an ideal yaw rate.

Hammad and He proposed the LQR-based controller to track a reference yaw rate [30]. Figure 2.11 illustrates the LQR control scheme in terms of a block diagram.

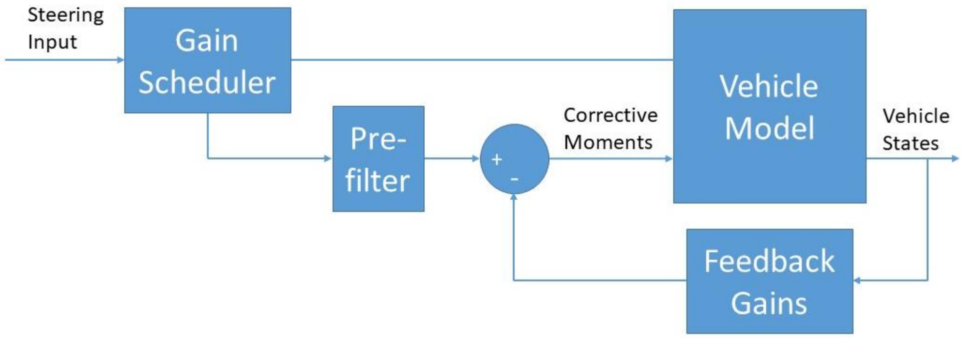

Figure 2.10: The combined full state feedback and open-loop prefilter control strategy [21].

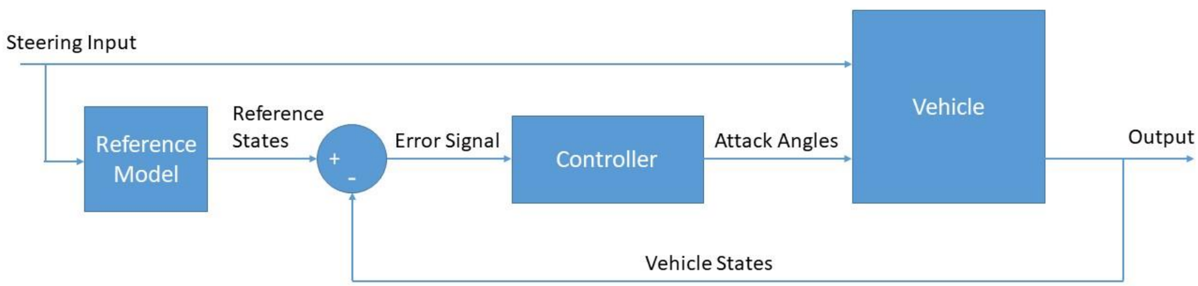

Figure 2.11: The LQR control scheme proposed in Ref. [30].

Diba et al. designed a rather unorthodox control system. The control objective was simplified to compensating the load transfer of the vehicle, which in turn affects the vehicle states [3, 22]. The control system consists of two layers. The system states are estimated, the required normal forces are calculated, and then the attack angles of the four wings required to generate these forces are chosen in the first layer. The second layer of the control system consists of a PID controller to move the actuators so as to rotate the wings by the given angle of attack. As shown in Figure 2.12, lookup tables were used to choose the needed attack angles [29]. These tables were formed using extensive CFD simulations of a wing.

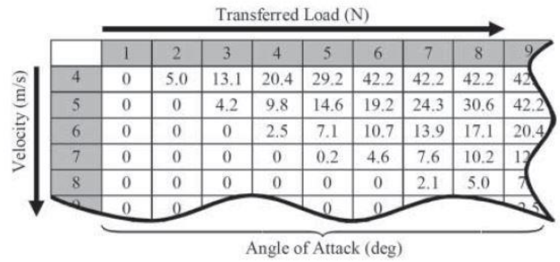

Transferred Load (N)

Velocity (m/s)

	1	2	3	4	5	6	7	8	9
4	0	5.0	13.1	20.4	29.2	42.2	42.2	42.2	42
5	0	0	4.2	9.8	14.6	19.2	24.3	30.6	42.2
6	0	0	0	2.5	7.1	10.7	13.9	17.1	20.4
7	0	0	0	0	0.2	4.6	7.6	10.2	12
8	0	0	0	0	0	0	2.1	5.0	7
[illegible]	0	0			0	0			

Angle of Attack (deg)

Figure 2.12: A lookup table used in an AAD control system [29].

The first lookup table is used to generate the required angles of attack of the wings to achieve the desired lateral load transfer at the current forward speed. The respective values of the attack angle and the transferred load are calculated using a series of CFD simulations and vehicle dynamic equations. In the second lookup table, the aerodynamic forces are calculated as a function of the vehicle forward speed and the attack angles. Thus, the AAD system is designed based on two lookup tables built upon a large number of simulation results. Ahangernejad and Melzi also followed a similar strategy with some improvements in the overall design [4]. For the control objective, reference normal load variables were tracked.

The LQR technique is a well-established control algorithm to design optimal controllers for active aerodynamic systems. Once the design objective and constraints are reasonably considered and established, the resulting LQR-based AAD controller may ensure the expected performance and guarantee the stability of the active aerodynamic system [21, 30]. The LQR-based AAD controller was designed using a linear vehicle model. Thus, the applicability of the LQR-based AAD controller under an evasive maneuver at high lateral accelerations, e.g., 0.8g, is questionable. Moreover, in the design of the LQR-based controller, it is assumed that all vehicle system parameters, e.g., vehicle forward speed and payload, are constant. Thus, the robustness of the LQR-based AAD subjected to external disturbances, such as side wind, is doubted.

The traditional PID control technique has been applied for the design of the AAD controller [3, 22]. This conventional control technique has been widely used in various applications, and the respective controller designs are relatively easy to be implemented. However, the control gains are generally determined using the trial and error method, and the resulting controllers cannot guarantee the stability of the systems. Moreover, the desired active aerodynamic control system should be robust, subjected to vehicle system uncertainties, varying operating conditions, and external disturbances. Unfortunately, the published PID-based AAD controllers did not adequately consider the aforementioned uncertainties.

Therefore, a model-independent controller will be explored in this thesis based on a sliding mode control (SMC) technique, which is robust in nature and is applicable to nonlinear systems. The SMC technique is a control method, in which the dynamics of a system is altered to follow the desired trajectory in its state space. The SMC implementation is often based on an error signal between the desired state and the actual state [35, 36].

2.5 Summary

The past two decades have witnessed the increasing research efforts on active aerodynamic control systems. The published research results indicate that for high-speed road vehicles, active aerodynamic control systems can significantly improve the longitudinal, vertical, and lateral dynamics. In addition to the streamlined body design, active aerodynamic surfaces can further reduce the aerodynamic drag to improve the acceleration performance of the vehicle and fuel economy. It is well-known that in road vehicle suspension design, there is a trade-off between ride quality and tire road holding capability. Active aerodynamic control provides an effective way to relieve the trade-off by adaptively varying the downforce of tires. It is shown that coordinating the active aerodynamic and active suspension actuators can greatly improve ride quality without degrading road holding capability. Moreover, by means of increasing the downforce of tires and adaptively adjusting axle load distributions, vehicle handling and lateral stability can be enhanced. Some research efforts have been made on examining the effects of active aerodynamic control on drag and downforces.

Various vehicle models with different complexity and fidelity were developed for exploring active aerodynamic control systems. For the purpose of numerical simulation, the vehicle models have been derived with high complexity and fidelity, while to design aerodynamic controllers, the objective-oriented vehicle models with less complexity and fidelity have been derived. A variety of control strategies have been proposed for active aerodynamic control, including PID, LQR, etc. These control strategies have been implemented with varying degrees of success. Interesting CFD simulations have been conducted to investigate the effects of varying the attack angles of spoilers and vehicle forward speeds on aerodynamic drags and downforces. The past studies on active aerodynamic control have paved the road for further development of techniques in this field.

Chapter 3

Vehicle System Models

A road vehicle is generally modelled as a multi-body dynamic system, which consists of a sprung mass (i.e., vehicle body) represented by a rigid or flexible body, multiple unsprung masses (namely, front and rear axles) represented by the respective rigid or flexible beams, and multiple pneumatic tires represented by springs and dampers. The sprung mass is connected to the unsprung masses by means of springs, dampers, and/or force actuators, which construct the conventional passive suspensions or active suspensions. With bearings, pneumatic tires are connected with an axle on the right and left end. To improve aerodynamic performance, various devices, e.g., rudders, spoilers or wings, etc., can be equipped on the vehicle body. The derivation of the equations of motion for all the components of a vehicle system and the contributing forces and moments, which describe the vehicle's dynamic behavior as a function of time, is referred to as vehicle modeling. It is a crucial and the first step towards designing a controller for a given vehicle system.

Road vehicles in the real world are generally highly nonlinear dynamic systems and, as a result, realistic models should be complex in nature. However, with appropriate assumptions, models can be simplified to varying extents. The simplicity depends upon the number of degrees of freedom, along which the motion of each of the components of the vehicle system is modeled. Another source of complexity is the inter-dependency of the vehicle states. Lastly, the modeling of different forces, which are due to tires, suspensions, and wings, etc., can be done in linear or nonlinear terms. Thus, the way they are modeled can also be a cause of complexity. Therefore, a number of vehicle models can be developed of varying intricacy depending on the need and requirements. Three vehicle models are used in this thesis:

i. 2-DOF single-track model
ii. 3-DOF nonlinear model
iii. 14-DOF CarSim model

This chapter introduces these models, explains their functionalities, and justifies their selection.

3.1 2-DOF Model

Figure 3.1 shows the 2-DOF model, i.e., a linear yaw-plane model frequently known as the bicycle model. The two motions considered are the lateral motion and the yaw motion of the vehicle. This model is used to generate a reference yaw rate as the tracking objective of the controller [18]. This vehicle model reflects the desired relationship between steering input and the vehicle yaw rate. By means of tracking the reference yaw rate, the dynamics of the vehicle is forced to the linear dynamic range, where the vehicle is stable and controllable.

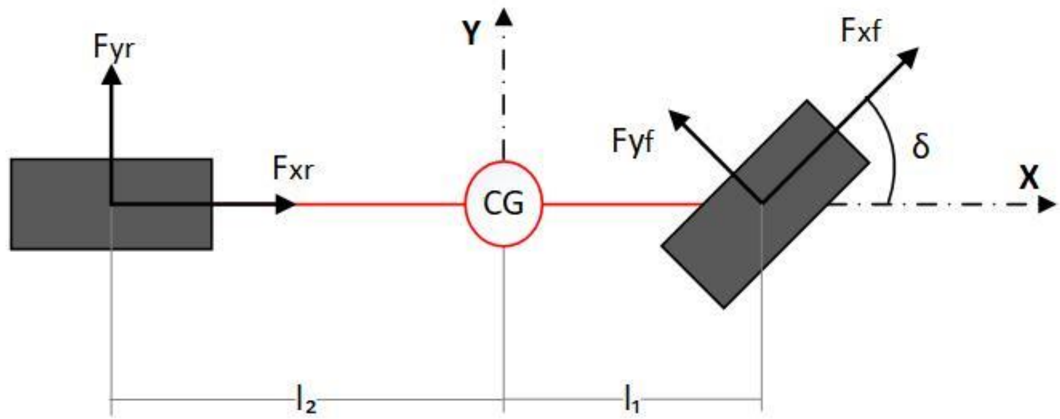

Figure 3.1: Schematic of a 3-DOF yaw-plane linear bicycle model.

Based on this model, the equation for the steady-state yaw rate can be written as follows.

$$r_{ss} = \frac{u}{l + \frac{K_{us}u^2}{g}}\delta \tag{3.1}$$

where,

$$K_{us} = \frac{Mgl_2}{2lC_f} - \frac{Mgl_1}{2lC_r} \tag{3.2}$$

Equation (3.1) is a function of the driver's steer input, which reflects the driver's intention [38]. But it must be limited by a function of the tire-road adhesion coefficient. Therefore, the target yaw rate with the consideration of the tire-road adhesion coefficient can be expressed as [39]

$$r_t = \begin{cases} r_{ss} & if \quad r_{ss} \leq {0.85\mu g}/{u} \\ {0.85\mu g}/{u} & if \quad r_{ss} > {0.85\mu g}/{u} \end{cases} \tag{3.3}$$

3.2 3-DOF Model

The 3-DOF model is a nonlinear model with the sprung mass roll motion as an additional DOF compared to the 2-DOF model introduced in Section 1.1. This model is used to simulate the dynamics of the vehicle, and thus assesses the performance of the AAD controller, which will be designed in Chapter 4, by measuring and recording various vehicle states. The actual yaw rate to be controlled, which acts as an input to the controller, is also generated by this model.

The use of this model is warranted because aerodynamic effects are manifest only at high speeds. At high speeds, the dynamics of the vehicle, especially the dynamics of the tires, enter into nonlinear dynamic range. Since the yaw rate is primarily a function of the tire forces, its actual value at high speeds will not be accurate if estimated based on the linear tire model. This may lead to an inaccurate input to the controller, thereby resulting in an erroneous control signal in terms of the attack angles.

This model is featured with a good trade-off between simplicity and accuracy. It is simple enough to facilitate the study of aerodynamic effects. It is accurate enough to capture the necessary dynamic features of the vehicle in evaluating the safety of the vehicle. Moreover, it is also cost-effective and computationally efficient.

The yaw-plane dynamics is shown in Figure 3.2. The figure also presents important dimensions that are influential in the vehicle's response. The modeling is based upon the ISO vehicle coordinate system [31].

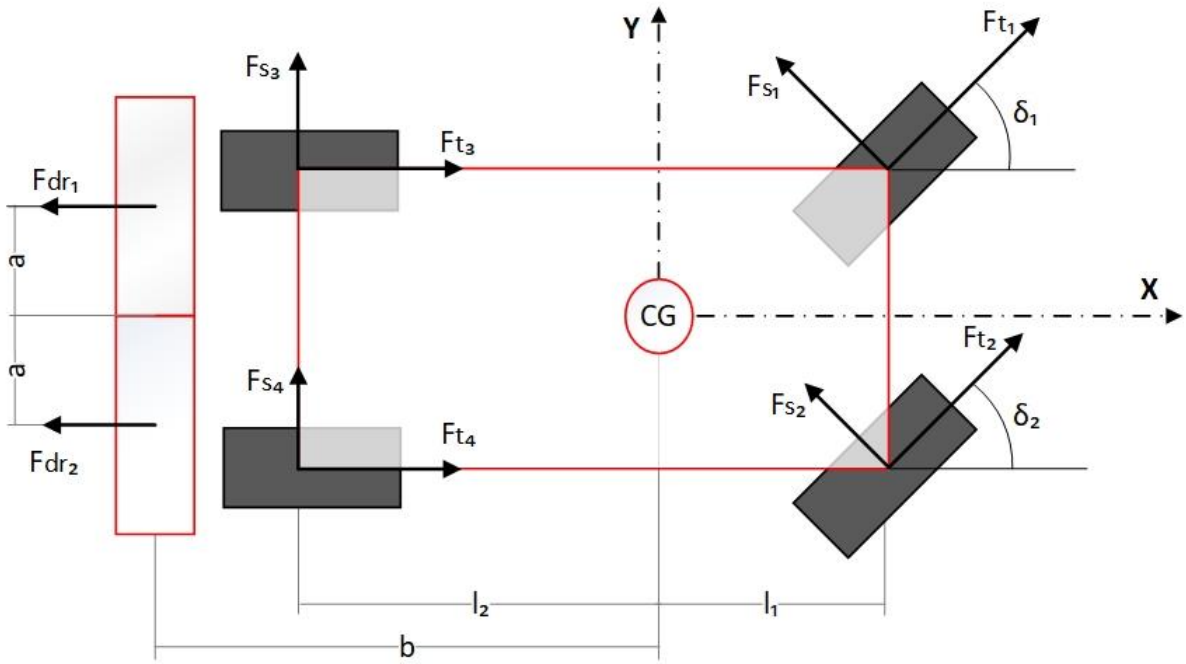

Figure 3.2: Schematic representation of the yaw-plane dynamics of the 3-DOF vehicle model.

$$\dot{v} = \frac{1}{m}\left(\sum_{i=1}^{4} F_{yi} - mur\right) \tag{3.4}$$

$$\dot{r} = \frac{1}{I_{zz}}\left(\frac{T}{2}\left(\sum_{i=2,3} F_{xi} - \sum_{i=1,4} F_{xi}\right) + l_1 \sum_{i=1,2} F_{yi} - l_2 \sum_{i=3,4} F_{yi} + a\left(F_{dr_1} - F_{dr_2}\right)\right) \tag{3.5}$$

The above equations represent the lateral motion and yaw motion of the vehicle, respectively. The vehicle forward speed is assumed as a constant.

Figure 3.3 illustrates the roll dynamics of the vehicle body as observed from the rear end of the vehicle.

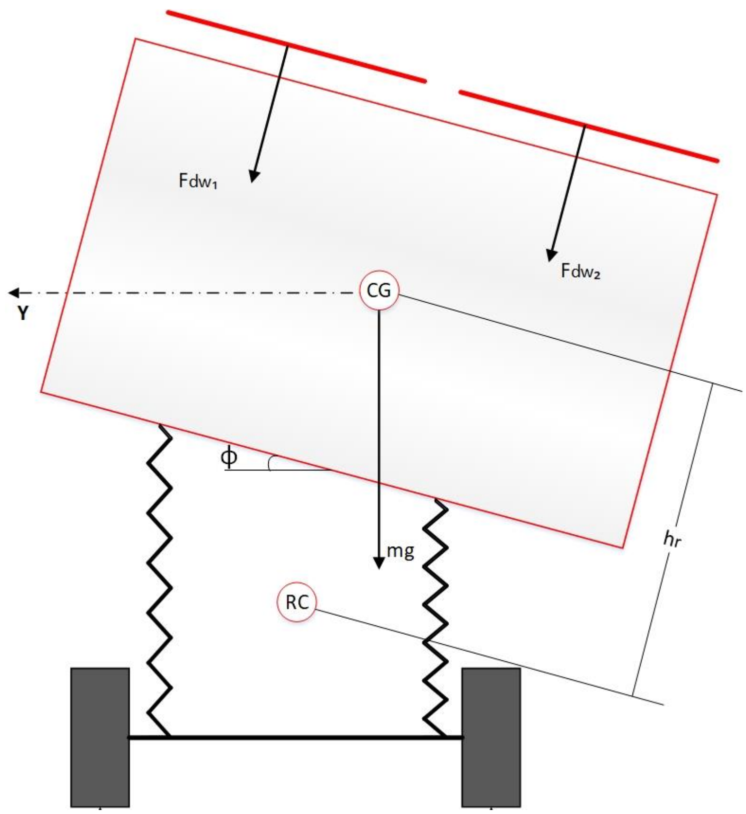

Figure 3.3: Schematic representation of the roll dynamics of the 3-DOF vehicle model.

$$\dot{p} = \frac{1}{I_{xx}}\big(a\big(F_{dw_2} - F_{dw_1}\big) - K_r \cos\varphi - C_r \cos\varphi - m_s \dot{v} h_r \cos\varphi - m_s u h_r r \cos\varphi + m_s g h_r sin\varphi\big) \tag{3.6}$$

Equation (3.6) represents roll motion of the vehicle's sprung mass. The overall spring stiffness and the damping coefficient is given

$$K_r = \sum_{i=1}^{4}\left(K_i \frac{T}{2}\sin\varphi\right)\left(\frac{T}{2}\right) \quad ; \quad C_r = \sum_{i=1}^{4}\left(C_i \frac{d}{dt}\left(\frac{T}{2}\sin\varphi\right)\right)\left(\frac{T}{2}\right) \tag{3.7}$$

The tire forces in equations (3.4) and (3.5) can be divided into components of the tractive and side forces generated by the lateral and longitudinal slip of the tire components, respectively.

$$F_{xi} = F_{ti}cos\delta - F_{si}sin\delta \;\; ; \; F_{yi} \; = F_{si}cos\delta + F_{ti}sin\delta, \;\; \mathrm{i} = 1{,}2{,}3{,}4 \tag{3.8}$$

The general equations for the drag and downforce were discussed in Chapter 2. As the wings rotate through an angle, the wind attacking the wings generates different forces as the angles vary. The aerodynamic forces in these circumstances can be modeled as

$$F_{dr_\mathrm{i}} = \frac{C_{dr_i}\rho A_{dr_i}u^2}{2}, \;\; i = 1{,}2 \tag{3.9}$$

$$F_{dw_\mathrm{i}} = \frac{C_{dw_i}\rho A_{dw_i}u^2}{2}, \qquad \mathrm{i} = 1{,}2 \tag{3.10}$$

The above equations will be elaborated in the next section.

The tractive and side forces in equation (3.8) are estimated using the well-known Magic Formula tire model [40].

$$(F_{ti}, F_{si}) = f(F_{zi}, \alpha_i, \kappa_i, \gamma_i) \tag{3.11}$$

As it is explicit in the above equation, the tire forces are a function of the normal load on the tires, the slip angles, the longitudinal slip ratios, and the camber angle. The normal loads, which are a function of the roll angles, lateral velocity and the location of the CG and the rear wings, can be calculated as

$$\begin{aligned} F_{z_1} = \frac{M_s g l_2}{2l} - \frac{M_s v l_2}{l}\frac{h_{12}}{T}\cos\varphi + \frac{M_{uf}g}{2} + \frac{M_{uf}h_{front}\dot{v}}{T} \\ - \left[K_1\left(\frac{T}{2}\sin\varphi\right) + C_1\left(\frac{T}{2}\cos\varphi\right)\right] - F_{l1}\left(\frac{b - l_2}{l}\right) \end{aligned} \tag{3.12}$$

$$F_{z_2} = \frac{M_s g l_2}{2l} + \frac{M_s v l_2}{l}\frac{h_{12}}{T}\cos\varphi + \frac{M_{uf} g}{2} + \frac{M_{uf} h_{front} \dot{v}}{T} + \left[K_1\left(\frac{T}{2}\sin\varphi\right) + C_1\left(\frac{T}{2}\cos\varphi\right)\right] - F_{l2}\left(\frac{b - l_2}{l}\right) \tag{3.13}$$

$$F_{z_3} = \frac{M_s g l_1}{2l} - \frac{M_s v l_1}{l}\frac{h_{34}}{T}\cos\varphi + \frac{M_{ur} g}{2} - \frac{M_{ur} h_{rear} \dot{v}}{T} - \left[K_3\left(\frac{T}{2}\sin\varphi\right) + C_3\left(\frac{T}{2}\cos\varphi\right)\right] + F_{l1}\left(\frac{b + l_1}{l}\right) \tag{3.14}$$

$$F_{z_4} = \frac{M_s g l_1}{2l} - \frac{M_s v l_1}{l}\frac{h_{34}}{T}\cos\varphi + \frac{M_{ur} g}{2} + \frac{M_{ur} h_{rear} \dot{v}}{T} + \left[K_4\left(\frac{T}{2}\sin\varphi\right) + C_4\left(\frac{T}{2}\cos\varphi\right)\right] + F_{l2}\left(\frac{b + l_1}{l}\right) \tag{3.15}$$

The slip angles are calculated according to the geometry shown in Figure 3.4. Although the kinematics is shown in the bicycle model, the final equation for slip angle remains unchanged from a double track model.

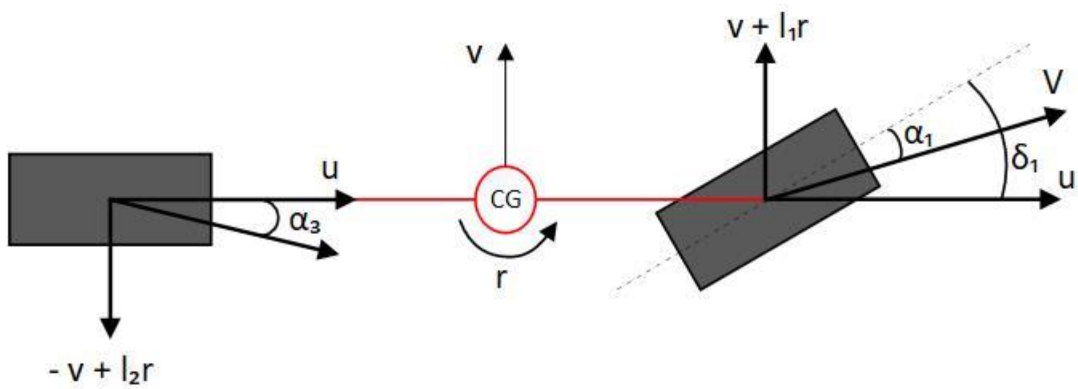

Figure 3.4: Kinematics of the tires and the CG of a vehicle.

For the front tire, we have

$$\tan(\delta_1 - \alpha_1) = \frac{(\mathrm{v} + l_1\mathrm{r})}{\mathrm{u}}$$

$$\delta_1 - \alpha_1 = \tan^{-1}\left(\frac{(\mathrm{v} + l_1\mathrm{r})}{\mathrm{u}}\right)$$

$$\alpha_1 = -\delta_1 + \tan^{-1}\left(\frac{(v + l_1 r)}{u}\right) \tag{3.16}$$

For the rear tire, the following relations hold,

$$\tan\alpha_3 = \frac{-\mathrm{v} + l_2\mathrm{r}}{\mathrm{u}}$$

$$\alpha_3 = -\tan^{-1}\left(\frac{-v + l_2 r}{u}\right) \tag{3.17}$$

Similarly,

$$\alpha_2 = -\delta_2 + \tan^{-1}\left(\frac{(v + l_1 r)}{u}\right) \tag{3.18}$$

$$\alpha_4 = -\tan^{-1}\left(\frac{-v + l_2 r}{u}\right) \tag{3.19}$$

Since the forward speed is assumed as a constant, this means there is no acceleration or braking. Thus, it can be assumed that the slip ratios are constant and, again, due to no compliance effects, the camber angle is assumed constant as well.

The inputs to this model are the steering-wheel angle and the attack angles of the rear wings. The steering-wheel angle is converted to the front wheel steering angles according to the steering configuration as follows,

$$\delta_1 = \delta_{sw}(R_{rp})(R_s)(R_{sr});\ R_{sr} = \begin{cases} R_{rsr} & , \quad \delta_{sw}(R_{rp})(R_s) > 0 \\ R_{lsr} & , \quad \delta_{sw}(R_{rp})(R_s) < 0 \end{cases} \tag{3.20}$$

$$\delta_2 = \delta_{sw}(R_{rp})(R_s)(R_{sr});\ R_{sr} = \begin{cases} R_{lsr} & , \quad \delta_{sw}(R_{rp})(R_s) > 0 \\ R_{rsr} & , \quad \delta_{sw}(R_{rp})(R_s) < 0 \end{cases} \tag{3.21}$$

The values of the vehicle model parameters are offered in the Appendix. This model is derived and simulated in the MATLAB/Simulink environment.

3.3 CarSim Model

The CarSim model is generated using the CarSim software package. It is a three-dimensional (3D) nonlinear model, in which the following motions are considered: the sprung mass is considered as a rigid body with six DOF, namely the lateral, longitudinal, vertical, pitch, roll, and, the yaw motions, while the forward speed of the vehicle is assumed to remain constant under any maneuver. Besides, the spinning motions of the four tires, as well as the roll and bounce of the front and rear axles are also considered in the CarSim. Moreover, the suspension effects are also taken into account in the CarSim model. Thus, the CarSim model is a nonlinear 14-DOF model.

The CarSim model has been validated with numerical and experimental data, its co-simulation with the controller designed in Simulink is used to validate the controller design. The validation is implemented under specified maneuvers in the CarSim software package.

The CarSim software package is based on a symbolic multi-body program, namely VehicleSim (VS) Lisp, which is used to generate equations of motion for three-dimensional (3D) multi-body vehicle systems [41]. The description of the vehicle configuration is fed to VS Lisp, in terms of the number of DOF, location of the CG and the axles, suspension properties, etc., to generate the equations of motion in the form of ODEs. It transforms the ODEs into a computer language, e.g., C or FORTRAN to solve the equations. The CarSim software package involves the following three relevant elements, the VS browser, the CarSim databases, and the VS solver.

The VS browser is a graphical user interface, which serves as the primary interface to CarSim. The CarSim databases contain datasets of the system parameters, the tire-road interactions, the test maneuvers, etc. The datasets are to be selected based on the user's requirements. The VS solver is utilized to solve the relevant governing equations of motion of the vehicle model and to execute the defined dynamic simulations. The VS browser can be used to allow other applications, e.g. controller defined in Simulink and to access the CarSim databases via an interface.

It is important to mention that it is problematic to use the CarSim model as a direct replacement for the 3-DOF model because of these reasons:

1. The computational cost is high.
2. The aerodynamic wings are not available as components in the CarSim database, this raises the following problems:
    - It is difficult to explore the effects of aerodynamics.
    - The aerodynamic forces must be externally defined by the user and thus, the process is error-prone.

3.4 Rear Wing Model

The aerodynamic coefficients and the reference areas given in equations (3.9) and (3.10) are a function of the wing shape and the angle of attack. The aerodynamic coefficients for a single wing can be calculated by rearranging the formulas as

$$C_{dr_i} = \frac{2F_{dr_i}}{\rho A_{dr_i} u^2} \tag{3.22}$$

$$C_{dw_i} = \frac{2F_{dw_i}}{\rho A_{dw_i} u^2} \tag{3.23}$$

The aerodynamic forces are calculated by the numerical simulations using the CFD software, ANSYS Fluent. It is flexible to calculate reference areas based on different projections resulting in a different set of coefficient values. For this research, the reference area for the drag coefficient calculation is the area of the wing that blocks the wind in the horizontal direction as shown in Figure 3.5.

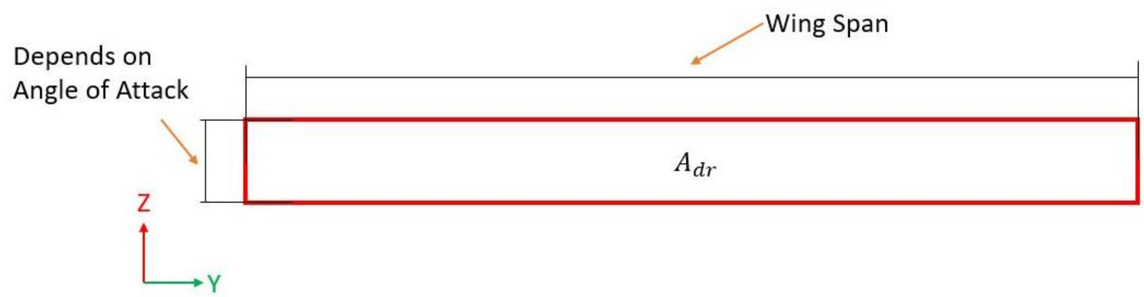

Figure 3.5: Reference area for the calculation of the drag coefficient with the wing at 0° *angle of attack.*

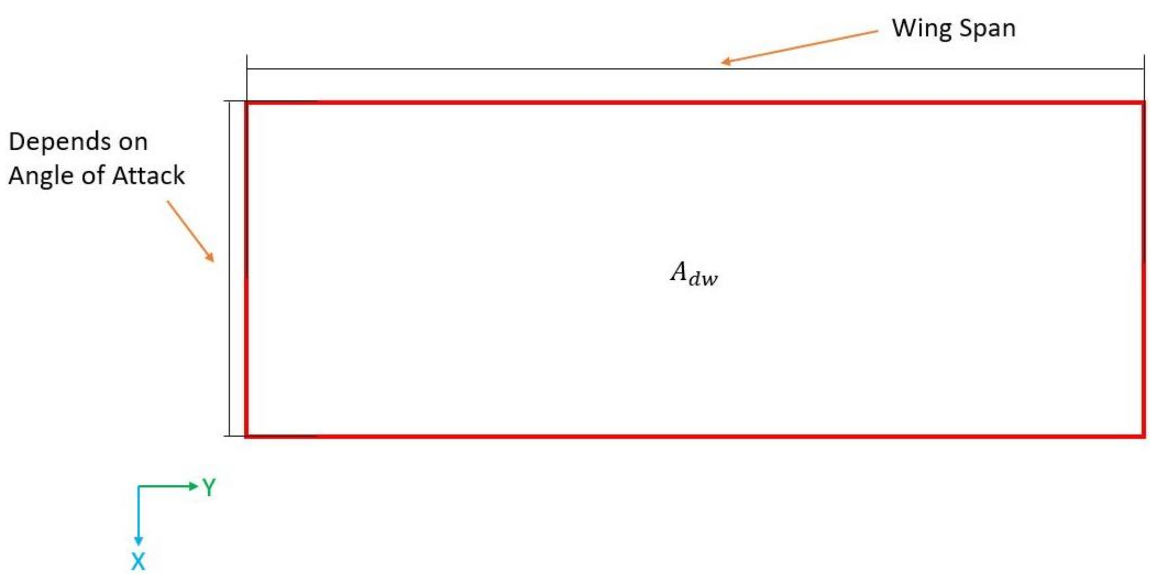

Figure 3.6: Reference area for the calculation of the downforce coefficient with the wing at 0° *angle of attack.*

The reference area for the downforce coefficient calculation is the planform area, i.e., the area of the wing as viewed from a bird's eye as shown in Figure 3.6.

These reference areas can be conveniently calculated by drawing projections of the wing at different angles. It can also be inferred that the reference areas in the two figures will exchange magnitudes as the angle of attack reaches 90°.

The shape of the wing should be selected based on the objective of the controller, which is mainly to increase the normal load on the concerned tires. Therefore, based on the past studies conducted in the author's lab [2, 23, 29], an airfoil shape with a high lift-to-drag ratio, i.e., Selig S1223, is chosen to model the rear wings. The planar coordinates for the said shape are sourced from the Ref. [42] and imported into the NX CAD software to design a 3D model of the wing as shown in Figures 3.7 and 3.8.

The CAD model is then imported into ANSYS Fluent software to simulate the aerodynamics and calculate the aerodynamic coefficients at various angles of attack. The blockage ratio is maintained under the value of 0.05 by keeping the boundaries of the virtual wind tunnel farther enough as shown in Figure 3.9.

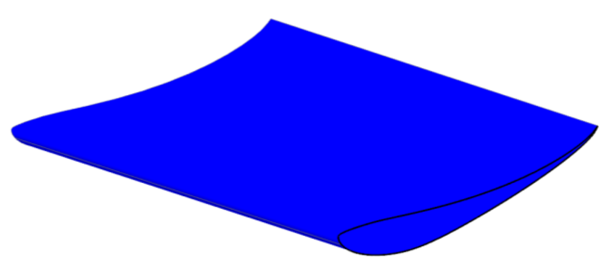

Figure 3.7: Isometric view of the rear wing design in NX CAD.

Figure 3.8: Side view of the rear wing design in NX CAD, showing the Selig S1223 profile.

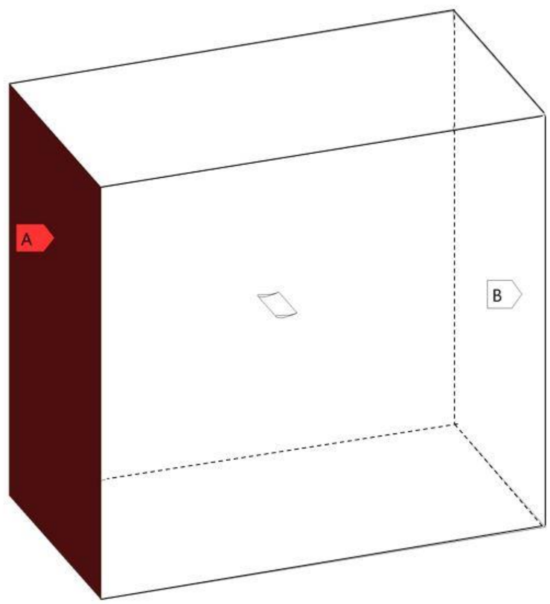

Figure 3.9: The virtual wind tunnel with face A as inlet, B as outlet and other four faces being the walls. Total length is 7.5 m, 4 m and 7 m along the X, Y and Z directions, respectively.

To ensure a good trade-off between the computation time and accuracy, the meshing operation is done repeatedly with increasing mesh size until the values of the lift coefficient seem to converge. Table 3.1 and Figure 3.10 present the data for these tests.

Table 3.1: Data from different mesh sizes and the simulations using those sizes to determine a reasonable mesh size.

	Number of elements in the mesh	Downforce (N)	ΔF_{dw} (N)
Trial 1	143003	194.3866	-
Trial 2	209838	203.4011	9.0145
Trial 3	268781	206.4066	3.0055
Trial 4	363293	209.1634	2.7568
Trial 5	481823	211.5047	2.3413
Trial 6	700334	212.6918	1.1871
Trial 7	1116930	213.8186	1.1268
Trial 8	1452485	214.4277	0.6091
Trial 9	1869176	214.219	-0.2087
Trial 10	2157974	213.9749	-0.2441

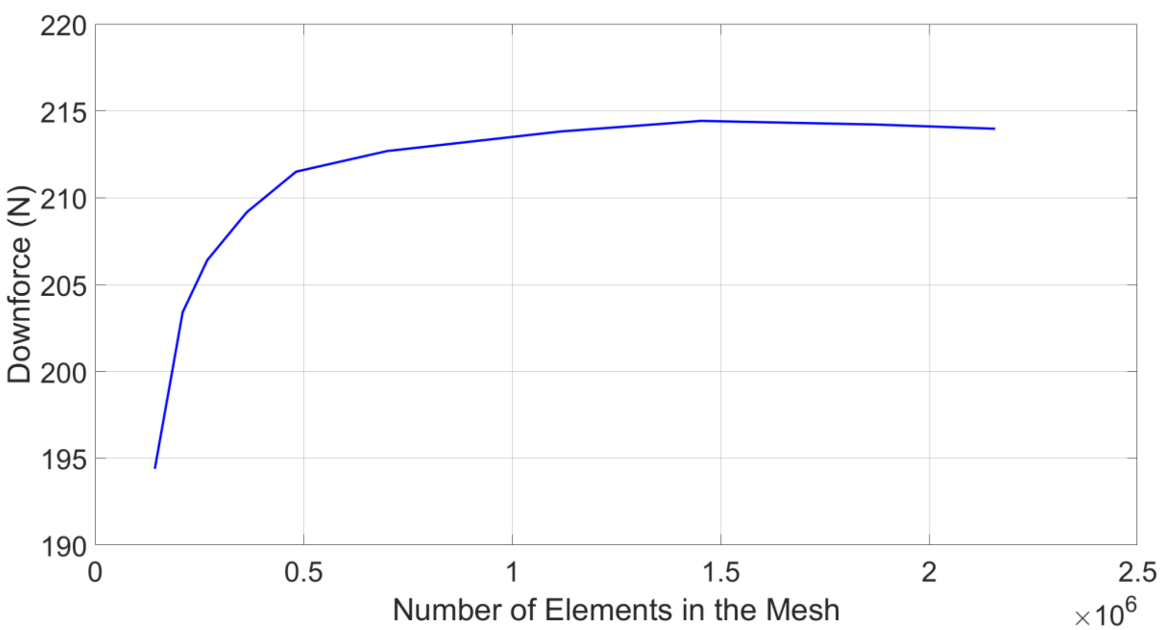

Figure 3.10: Mesh convergence test for the selected wing at 0° angle of attack.

Therefore, the mesh settings used to develop the mesh size at trial 6 are fixed for the rest of the simulations as there is no considerable change in the value of the drag coefficient on further refinement of the mesh size. Figures 3.11, 3.12, and 3.13 exhibit the mesh quality for three arbitrary trials.

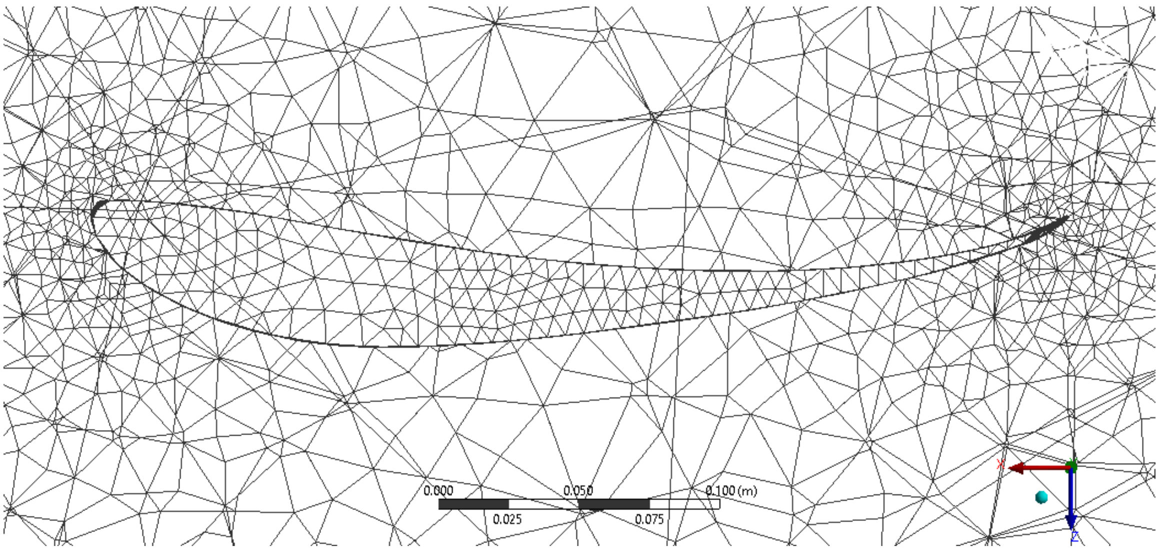

Figure 3.11: A cut section showing the mesh quality around the wing during trial-2.

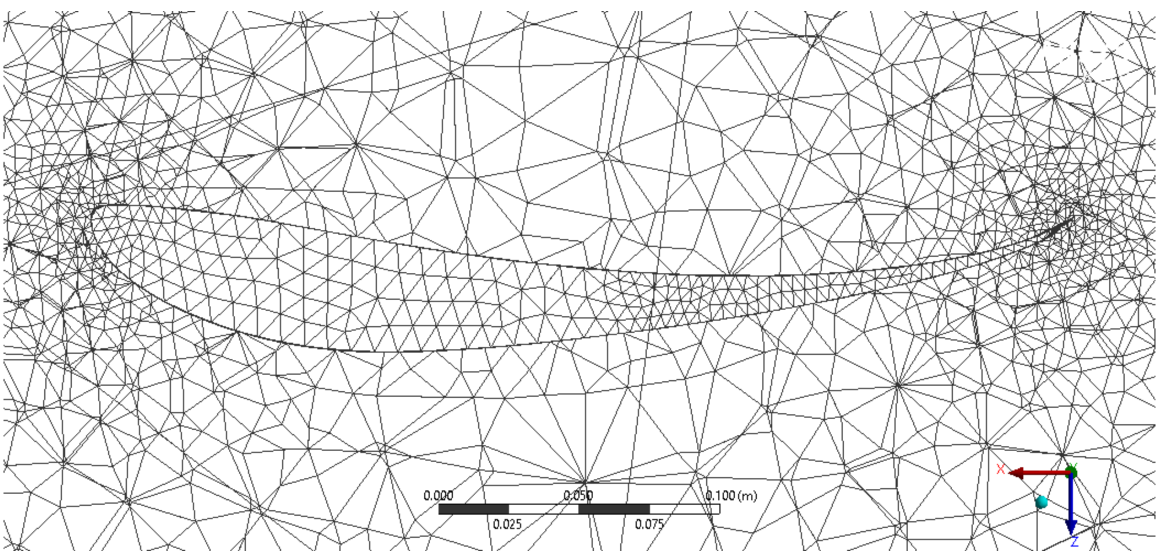

Figure 3.12: A cut section showing the mesh quality around the wing during trial-6.

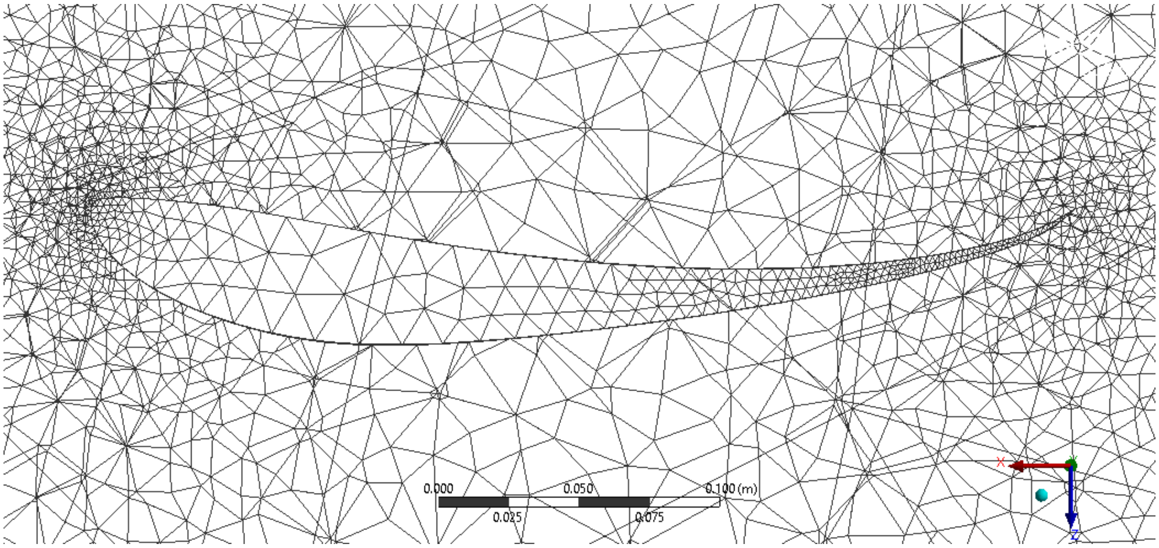

Figure 3.13: A cut section showing the mesh quality around the wing during trial-8.

The next step in acquiring the aerodynamic data is to set up the CFD problem appropriately. Shows the solver setting that were used in the following computations.

Table 3.2: Solver settings for CFD simulation.

Model	Realizable k-epsilon	
Boundary Conditions	Velocity Inlet	
	Magnitude	41.67
	Turbulent Intensity	1 %
	Turbulent Viscosity Ratio	10
	Pressure Outlet	
	Backflow Turbulent Intensity	5 %
	Backflow Turbulent Viscosity Ratio	10
Reference Values	Air Density	1.225 kg/m^3
Solution Method	Scheme	Coupled
	Momentum	2^{nd} Order Upwind
	Turbulent Kinetic Energy	2^{nd} Order Upwind
	Turbulent Dissipation Rate	2^{nd} Order Upwind

Solution Control	Flow Courant Number	50
	Explicit Relaxation factors	
	Momentum	0.25
	Pressure	0.25
	Under Relaxation Factors	
	Turbulent Kinetic Energy	0.8
	Turbulent Dissipation Rate	0.8
	Turbulent Viscosity	0.95
Solution Initialization	Hybrid	

Furthermore, the convergence of the lift forces as the solution progresses is also checked to assure the accuracy of the results as shown in Figure 3.14.

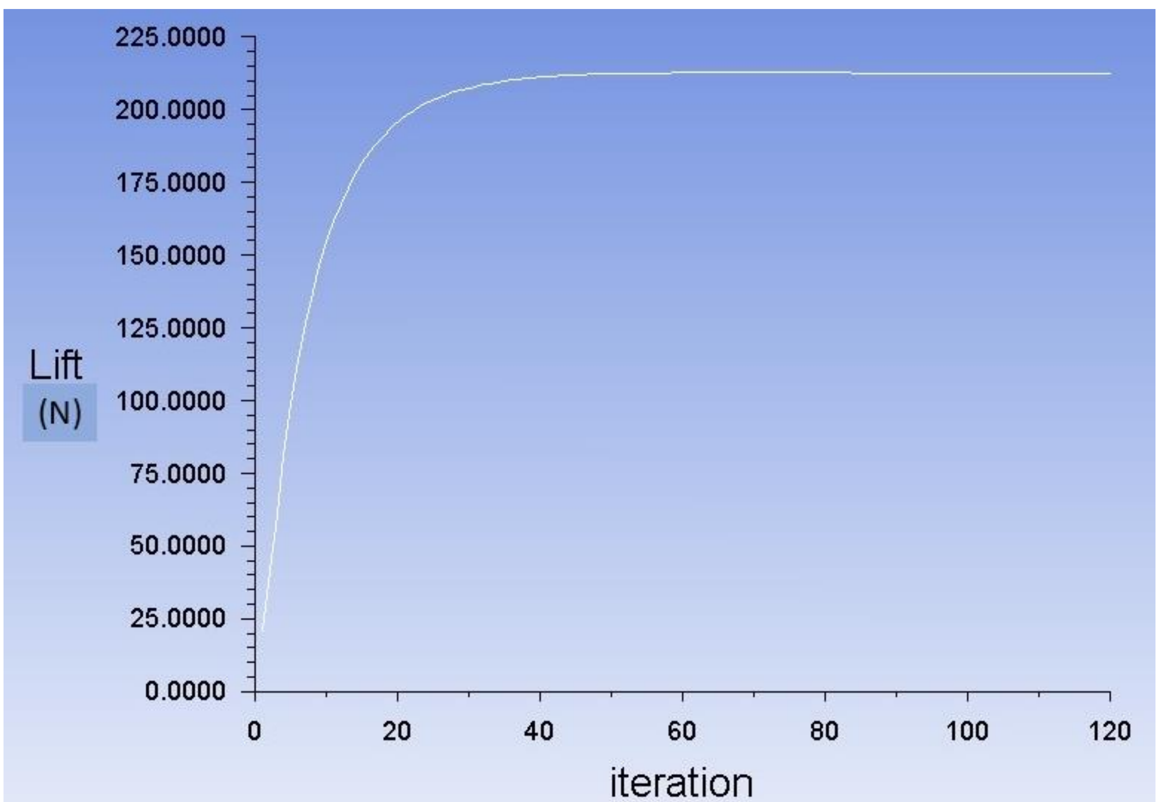

Figure 3.14: Convergence of the downforce as the solution progresses.

The observed downforce values at different attack angles are listed in Table 3.3. Table 3.3 also shows a peculiar observation at the angle of attack of 34°, after which there is a decline in the downforce because of 'flow separation' [43]. Figure 3.15 shows the variation of the downforce coefficient with the angle of attack.

Table 3.3: Aerodynamic coefficients of the modeled wing at different angles of attack.

Angle of Attack (deg)	Downforce (N)
0	212.6918
10	389.1453
20	533.966
30	643.3973
34	673.8328
40	521.9554
50	295.1735
60	204.7185
70	142.3279
80	78.1601
90	13.3739

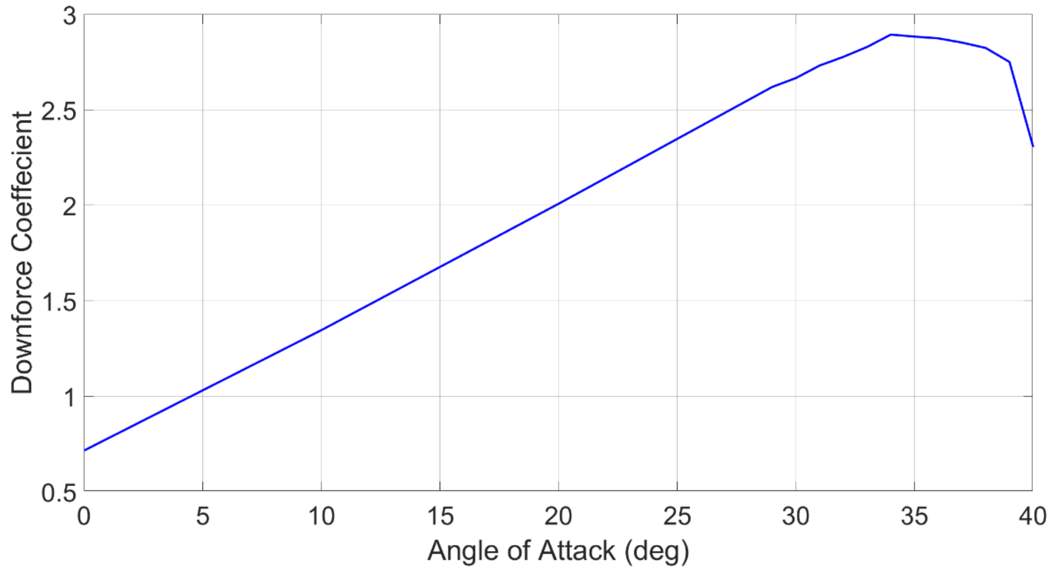

Figure 3.15: Variation of the downforce coefficient as the angle of attack is varied.

3.5 Summary

The 2-DOF linear yaw-plane model exhibits stable and controllable vehicle dynamics. Therefore, it has been presented to function as a reference for the controller. The use of aerodynamic aids is efficient when the vehicle runs at speeds above 80 km/h. At such speeds, even a very small steering input can take the dynamics of the vehicle into the nonlinear range. Hence, the derivation of a nonlinear model, rather than a linear one, is important and necessary. Hence, the equations representing a 3-DOF nonlinear model have been presented capturing all the influential dynamic motions yet neglecting and linearizing a few others to maintain a good balance between simplicity and accuracy. Figure 3.16 summarizes all the equations and shows their interconnections that make up the whole vehicle model.

As shown in Figure 3.16, the aerodynamic forces act as inputs to the vehicle model. The forces are modeled using equations (3.22) and (3.23) and the required aerodynamic coefficients are calculated based on CFD simulations on the CAD model of the wing.

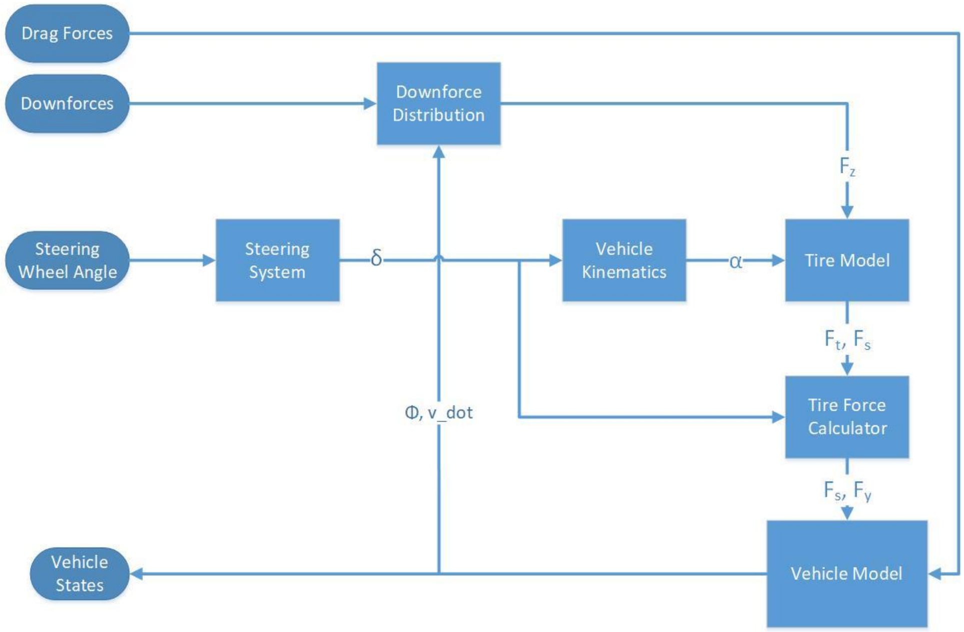

Figure 3.16: Block diagram of the dynamics of the vehicle.

These coefficients along with the respective reference area values are loaded in two separate lookup tables to convert the angles obtained from the controller into forces required by the vehicle model as shown in Figure 3.17.

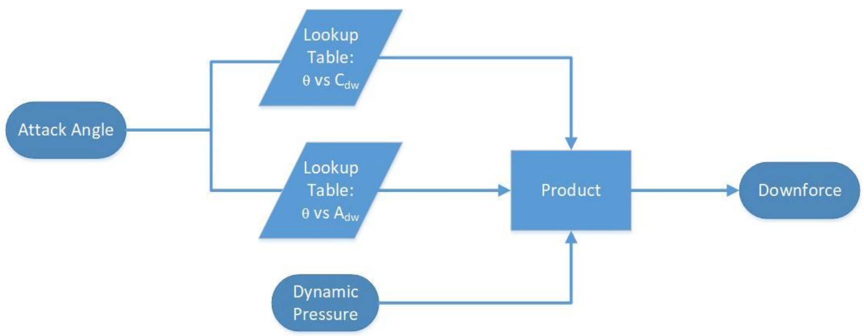

Figure 3.17: Block diagram for one of the wings showing the generation of the downforce.

Lastly, the CarSim software package is introduced and the three-dimensional vehicle body is generated to validate the controller design.

Chapter 4

Active Aerodynamic Control

The process of manipulating the position or orientation of aerodynamic devices, e.g., wings, spoilers, diffusers, etc. to influence the vehicle dynamic characteristics is known as active aerodynamic (AAD) control. The development of an AAD control system, like any other control system, comprises of two vital components: the control objective and the controller used to attain the decided objective(s).

The following sections present the tracking of a reference yaw rate as a control objective and the proposed sliding mode control (SMC), followed by simulations on MATLAB/Simulink to evaluate the performance of the vehicle equipped with AAD control.

4.1 Control Objective

The selection of a control objective is crucial, and it also affects the ease or difficulty, with which the controller is developed and implemented. Minimization of the vehicle sideslip angle, roll angle, roll rate, or the lateral load transfer, is usually considered as an objective for achieving better vehicle handling performance and lateral stability. However, forcing the yaw rate to resemble a steady-state cornering behavior encompasses most of the aforementioned objectives. The steady-state (reference) yaw rate is generated from the bicycle model as introduced in Chapter 3.

The controller takes the values of the actual and reference yaw rate, then compares them. If the reference value is less than that of actual, the controller tries to reduce the value of the actual one and vice versa. The control objective can be achieved in multiple ways and the following subsection explores them in detail.

4.1.1 Operating Modes

Yaw rate of a vehicle is primarily a function of tire forces. The vehicle body roll also affects but comparatively very less. The addition of the split rear wing adds more degrees of control for the yaw rate and there are three different ways the rear wings can be utilized to do so. These three operating modes assume that the reference yaw rate is less than the actual one, and the corrective yaw rate has to be applied in the opposite direction of the actual yaw rate.

The first mode is the action of a drag force couple of the right and left wings of the split rear wing, as shown in Figure 4.1. This is the only way that the rear wings affect yaw motion directly. The corrective moment generated by this couple is a function of the angle of attack of the two wings and distance of the point of action of drag force from the vehicle longitudinal centerline.

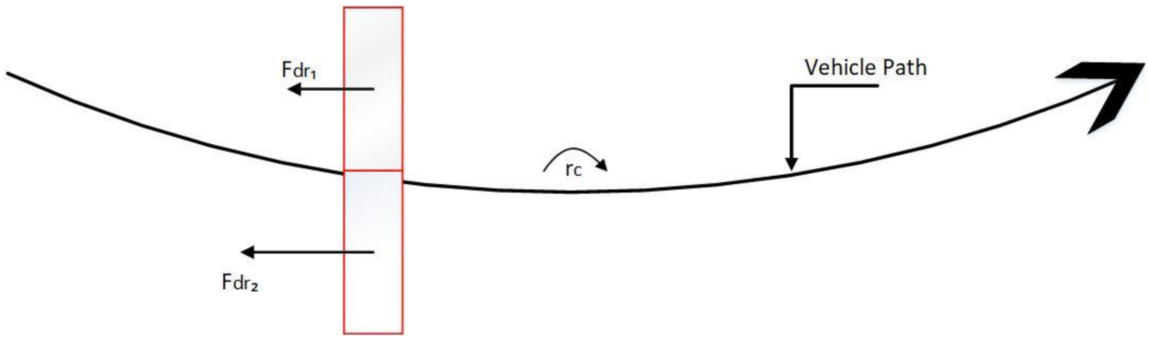

Figure 4.1: Schematic description of the first operating mode via a couple of the drag forces from the right and left wings of the split rear wing.

The second mode is the action of the couple formed by longitudinal forces generated by the rear tires, as seen in Figure 4.2. Since the longitudinal tire forces are a function of the regular normal loads and the downforces generated by the rear wings, the rear wings indirectly affect the yaw motion in this mode. The corrective yaw moment is also a function of the track width of the vehicle besides the angles of attack and the load transfer of the vehicle.

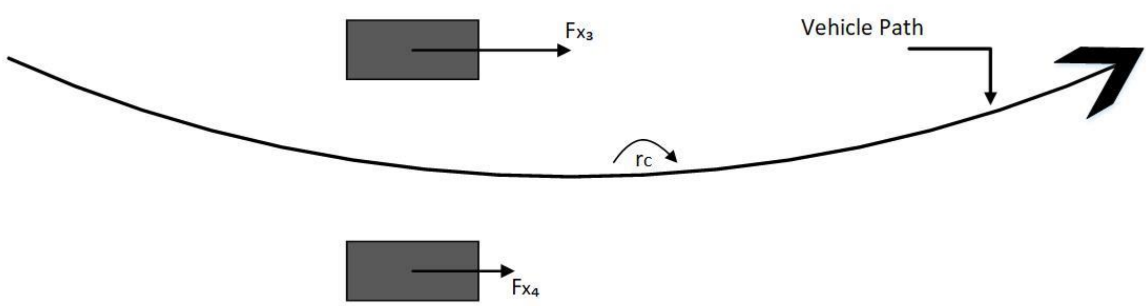

Figure 4.2: Schematic description of the second operating mode via a couple of the longitudinal forces from the two rear tires.

The action of the couple formed by the lateral forces on the front and rear axle is the third mode, as shown in Figure 4.3. This mode corresponds to the case where the rear wing acts as a single solid wing. Consequently, the angle of attack would be the same for both the right and left wings. The corrective moment, in this case, is a function of the axles' distance from the CG of the vehicle.

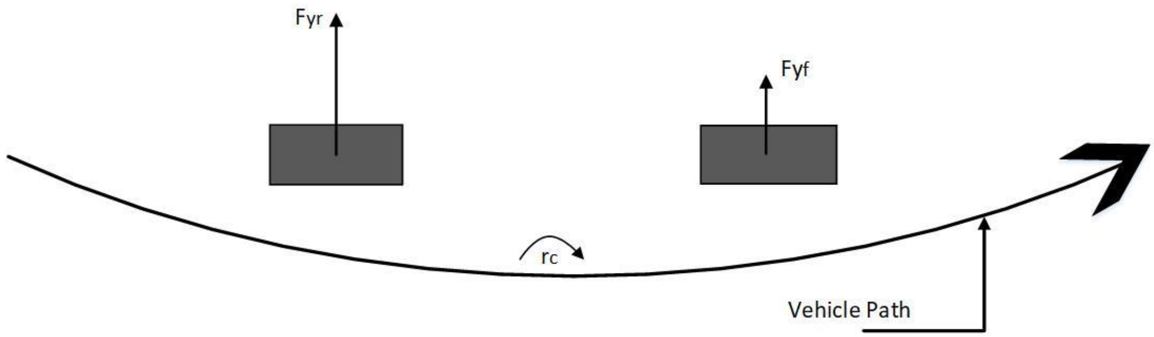

Figure 4.3: Schematic description of the third operating mode via a couple of the lateral forces from the front and rear axle's tires.

The requisite wing action for each of these modes to generate the required corrective yaw moment can be tabulated in Table 4.1.

Table 4.1: Requisite wing action for the three operating modes.

	Inner Wing	*Outer Wing*
Mode 1:	*Stay*	*Up*
Mode 2:	*Up*	*Stay*
Mode 3:	*Up*	*Up*

In the above table, 'Up' suggests that the angle of attack of the respective wing should increase to generate more drag and/or downforce, while 'Stay' means that the wing should be stationary. It can be understood that the needed wing action in modes 1 and 2 is diametrically opposite. A decision must be taken as to which of these modes should be undertaken to achieve the control objective. Since the wing design is based on an airfoil shape with a high lift to drag ratio, the downforce of this wing is more pronounced than the drag, at least at lower angles. It should be noted that in this research, the longitudinal tire forces are generated in terms of tractive forces due to the driving torque from the engine. Thus, in reality, mode 2 is more realistic than mode 1, and the latter will not be considered in the following chapters of the thesis. However, mode 1 is useful in studies based on linear models.

Another justification for selecting mode 2 is that it is partially synonymous with mode 3 in which both the wings needs raising. But mode 3 adversely affects the control objective when the reference yaw rate is more than the actual yaw rate because of the considerable downforce that is generated by the wings at their base position itself. In such cases, the operation of mode 2 can compensate for the negative effect of mode 3. Therefore, the selection of mode 2 is rational and applicable to all cases.

4.2 SMC Controller Design

Among a few control techniques that can be applied to nonlinear dynamical systems, a sliding mode control (SMC) approach is adopted to achieve the control objective. A sliding surface is designed based on the error signal so that the system slides along the surface until the error reaches zero.

The error function is defined as a difference between the actual yaw rate of the vehicle and the desired yaw rate, i.e. the steady-state yaw rate, given by Equation (4.1). The same error function is also designed as the sliding surface as expressed in Equation (4.2).

$$e = r_{ss} - r \tag{4.1}$$

$$\sigma = e \tag{4.2}$$

The appropriate control law chosen to stabilize the sliding surface is given as

$$\dot{\sigma} = -Usat\left(\sigma/_{E}\right) \tag{4.3}$$

where U and E are non-negative control parameters. The saturation function is used instead of the sign function to avoid the well-known chattering phenomenon at the cost of robustness. The controller, however, retains some of its robustness as demonstrated in Figure 4.15 and Table 4.2. The stability of the control system is ensured by selecting and evaluating a suitable Lyapunov Function.

The function is given by

$$L = \frac{1}{2}\sigma^2 \tag{4.4}$$

which leads to

$$\dot{L} = \sigma\dot{\sigma} \tag{4.5}$$

Combining Equations (4.2), (4.3), and, (4.5) we get

$$\dot{L} = -eUsat\left(\sigma/_{E}\right) \tag{4.6}$$

Since $U > 0$ and $E > 0$, and $\dot{L} \leq 0$. This indicates that a sufficient condition is satisfied for the stable sliding mode control.

Combining Equations (4.1), (4.2), and (4.3) we get

$$\dot{r}_{ss} - \dot{r} = -Usat\left(\sigma/_{E}\right) \tag{4.7}$$

The required aerodynamic forces for the control of the vehicle can be estimated by substituting Equation (3.2) into Equation (4.7) and rearranging the terms to solve for the aerodynamic forces.

Thus,

$$\frac{1}{I_{zz}}\left(\frac{T}{2}\left(\sum_{i=2,3} F_{xi} - \sum_{i=1,4} F_{xi}\right) + a\left(F_{dr_1} - F_{dr_2}\right) + l_1 \sum_{i=1,2} F_{yi} - l_2 \sum_{i=3,4} F_{yi}\right) - \dot{r} = -Usat\left({}^{\sigma}/_{E}\right) \tag{4.8}$$

As seen in Equation (4.8), only the aerodynamic drags are available. For operating mode 2, the downforces of the rear tires are primarily controlled by manipulating the angles of attack of the right and left wings of the split rear wing. Accessing the downforces in Equation (4.8) greatly increases the complexity and size of the equation, as well as the difficulty for its subsequent modeling on MATLAB/Simulink. It was also found that numerically solving this equation is time-consuming, costly, and thus, inefficient.

While analyzing the operation of the SMC controller based on the first operating mode, it was observed that the effect of all the other terms apart from the control law can be diminished by selecting appropriate values of the control parameters. Hence, a controller is designed in which the control input is merely a function of the control law.

$$Control\ Input = -Usat\left({}^{\sigma}/_{E}\right) \tag{4.9}$$

In this case, however, the control input is guided by externally defined laws to limit the action of the rear wings to physical limits and to ensure that the wings operate according to the needed objective. There are two such laws, which can be conveniently termed as governing equations. The governing equations also characterize the control input as the difference in the attack angles of the two wings that creates a corrective yaw moment.

The first governing equation can be given as

$$Control\ Input, (\theta_1 - \theta_2) = [-34°, 34°] \tag{4.10}$$

where 34° is the stall angle of the wing. The maximum attack angle of a wing is limited by its stall angle as shown in Equation (4.10). Positive attack angles are generated when the error is positive, i.e., when the desired yaw rate is larger than the actual yaw rate, and negative attack angles are generated when the error is negative.

Then the following governing equations distribute the attack angles as per the need to increase or decrease the vehicle's yaw rate and filter the negative angles.

$$\theta_1 = \begin{cases} -(\theta_1 - \theta_2), & (\theta_1 - \theta_2) < 0 \\ 0 \quad , & (\theta_1 - \theta_2) \geq 0 \end{cases} \tag{4.11}$$

$$\theta_2 = \begin{cases} (\theta_1 - \theta_2), & (\theta_1 - \theta_2) > 0 \\ 0 \quad , & (\theta_1 - \theta_2) \leq 0 \end{cases} \tag{4.12}$$

Lastly, the attack angles are converted to aerodynamic forces using the given relations and the aerodynamic data collected in Chapter 3.

The new controller is a major contribution of this thesis. The proposed SMC controller along with the selection of only one control objective simplifies the controller design greatly. It can also be seen that the controller is dependent on one state of the system, i.e. the yaw rate. It is expected that the proposed design method can be used to design a controller for any system with well-established dynamics.

4.3 Control System Analysis

Based upon the 3-DOF nonlinear model with the rear wings and the SMC-based AAD controller, numerical simulations are conducted in MATLAB. The simulations are performed using the vehicle model with and without the active aerodynamic system to analyze the performance of the AAD controller. The vehicle without the active aerodynamic system is also bereft of the passive rear wings because their presence can adversely affect the vehicle performance in some cases, as explained in the previous section. Moreover, the minimum test speed is 80 km/h because below this speed the influence of aerodynamics is not significant. The simulations are conducted under a given steering input. In addition to the open-loop dynamic simulations, closed-loop simulations, which are introduced in Chapter 5, are also performed, in which the driver attempts to follow a prescribed path. Without a driver model, the 3-DOF vehicle model derived in this research can only be used for open-loop simulations in MATLAB/Simulink. The open-loop simulations aim to evaluate the performance of the SMC-based AAD controller.

4.3.1 Steering Input

Figure 4.4 shows the front wheel steering input in terms of a single cycle sinewave with the amplitude of 0.03 rad and the frequency of 0.5 Hz.

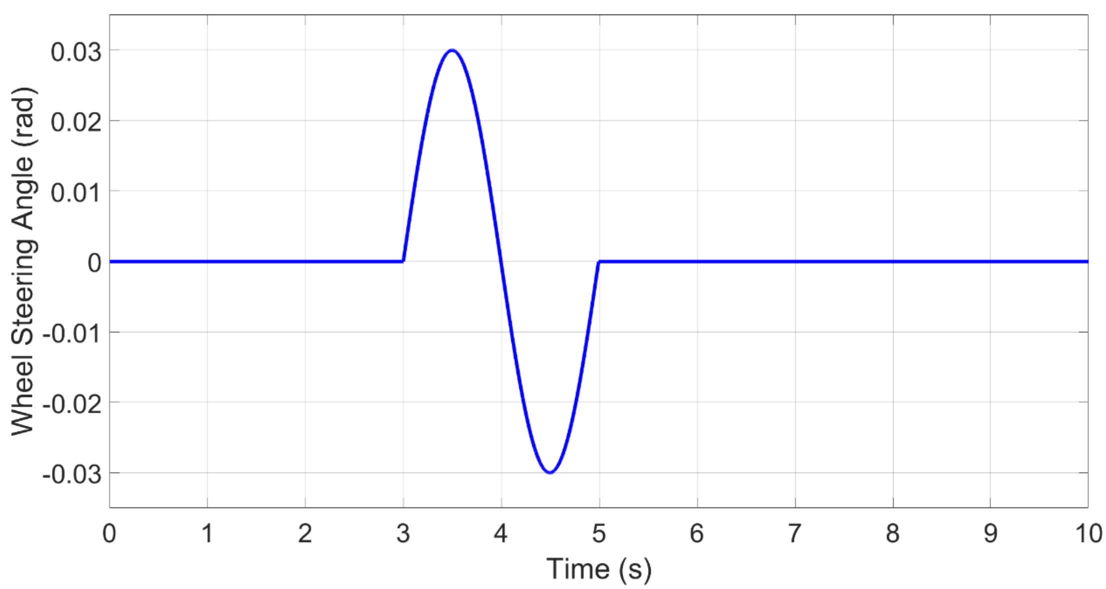

Figure 4.4: Time history of the front wheel steering input.

A positive steering angle means that a turn towards the left, and vice versa. It is expected that with the specified steering input and a given forward speed, the testing vehicle will execute a single lane-change maneuver.

4.3.2 Performance Enhancement due to AAD Control

Figure 4.5 shows the simulation result in terms of yaw rate response of the vehicle with and without AAD under the single lane-change maneuver at 120 km/h. It is observed that the peak values of the yaw rate drop due to the AAD control, implying that the lateral stability is enhanced. Figures 4.6 and 4.7 further confirm the improvement of the lateral stability of the vehicle with AAD control in terms of the side-slip angle and the lateral acceleration of the vehicle.

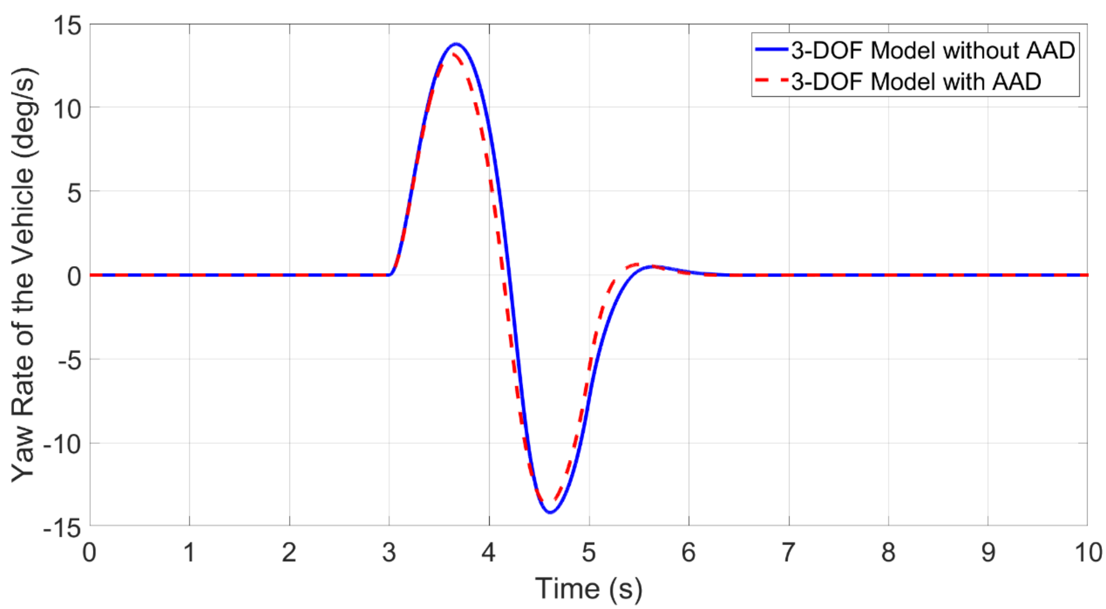

Figure 4.5: Time history of the yaw rates of the vehicle with and without the AAD system at 120 km/h.

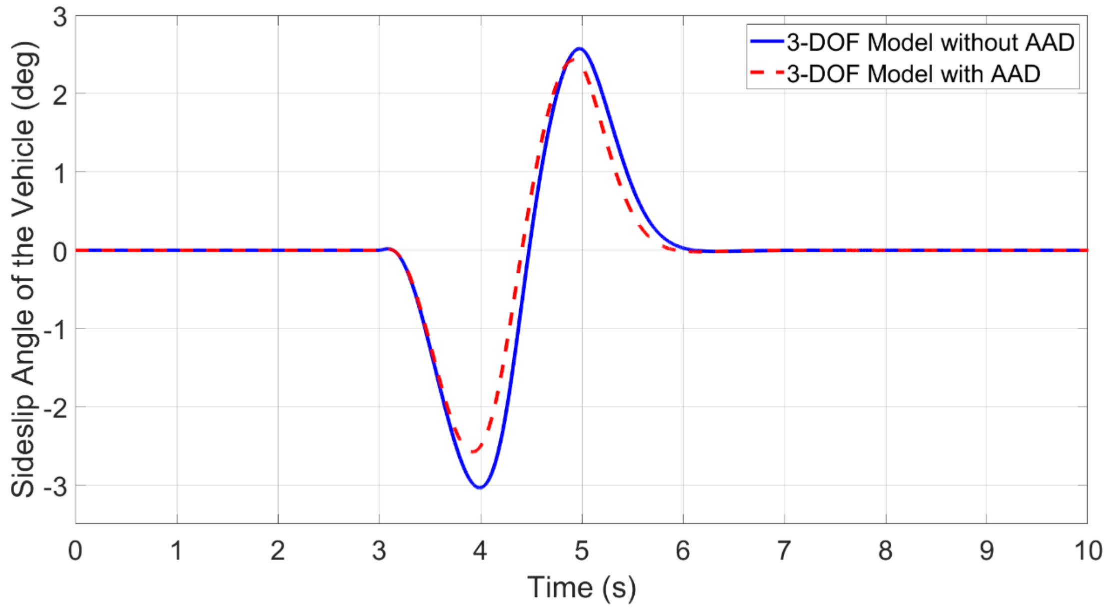

Figure 4.6: Time history of the side slip angles of the vehicle with and without the AAD system at 120 km/h.

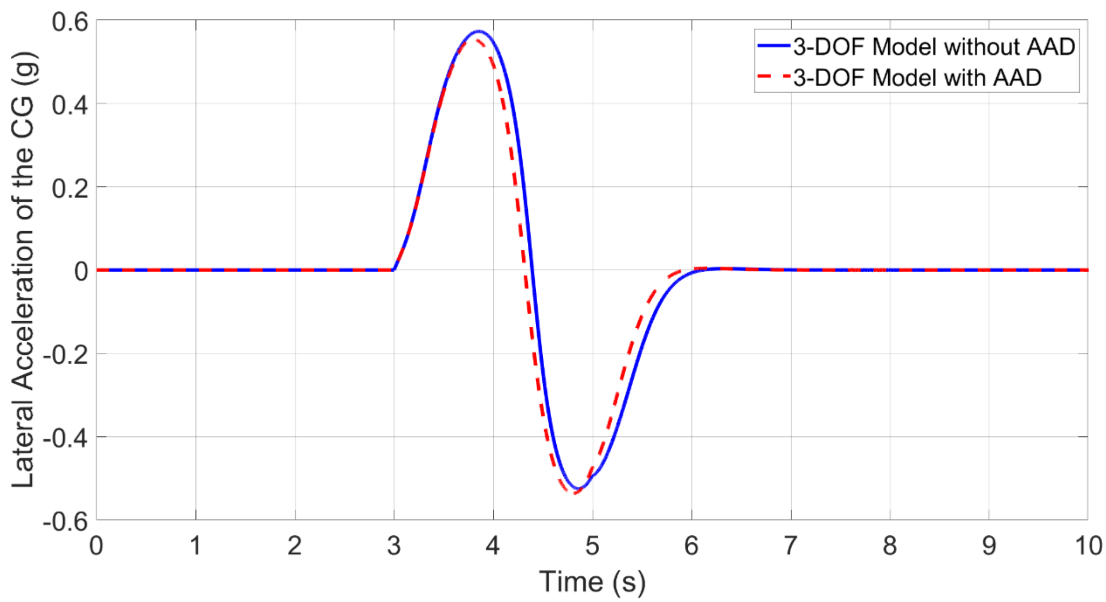

Figure 4.7: Time history of the lateral accelerations of the vehicle with and without the AAD system at 120 km/h.

Figure 4.8 illustrates the variation in normal loads on the rear tires. Note that for the case without AAD, the vehicle is not equipped with the wings. As shown in Figure 4.8, to decrease the yaw rate of the vehicle over the single lane-change maneuver, the controller makes the lateral load transformation smaller than the case without the controller.

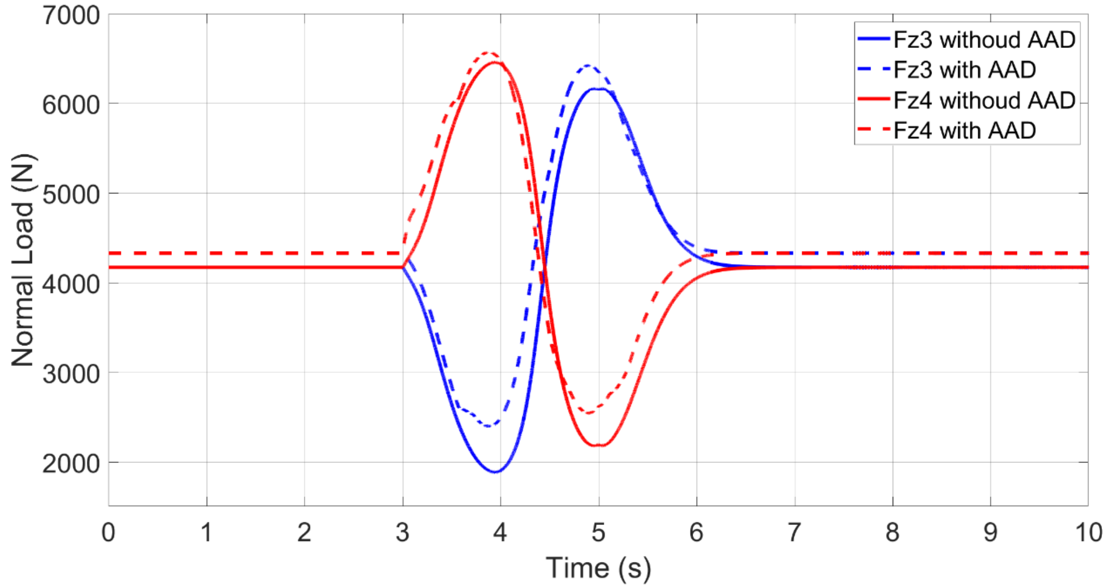

Figure 4.8: Time history of the normal loads acting on the rear tires of the vehicle with and without the AAD system at 120 km/h.

4.3.3 Effect of Speed Variation

Figures 4.9, 4.1, and 4.11 show the yaw rate responses of the vehicle with and without AAD control under the single lane-change maneuver at the speed of 80, 100, and 120 km/h, respectively. The change in yaw rate due to active aerodynamic control at 80 km/h is negligible, thus explaining its limitation at lower speeds. It is observed that as the vehicle forward speed increases, the effect of the controller becomes more evident. This is intuitive because the aerodynamic forces are proportional to the square of the vehicle speed. Figure 4.12 presents the time history of yaw rates of the vehicle with and without AAD control at the speed of 180 km/h. At this speed, the uncontrolled vehicle completely loses the yaw stability, while the controlled vehicle can settle back to a stable point.

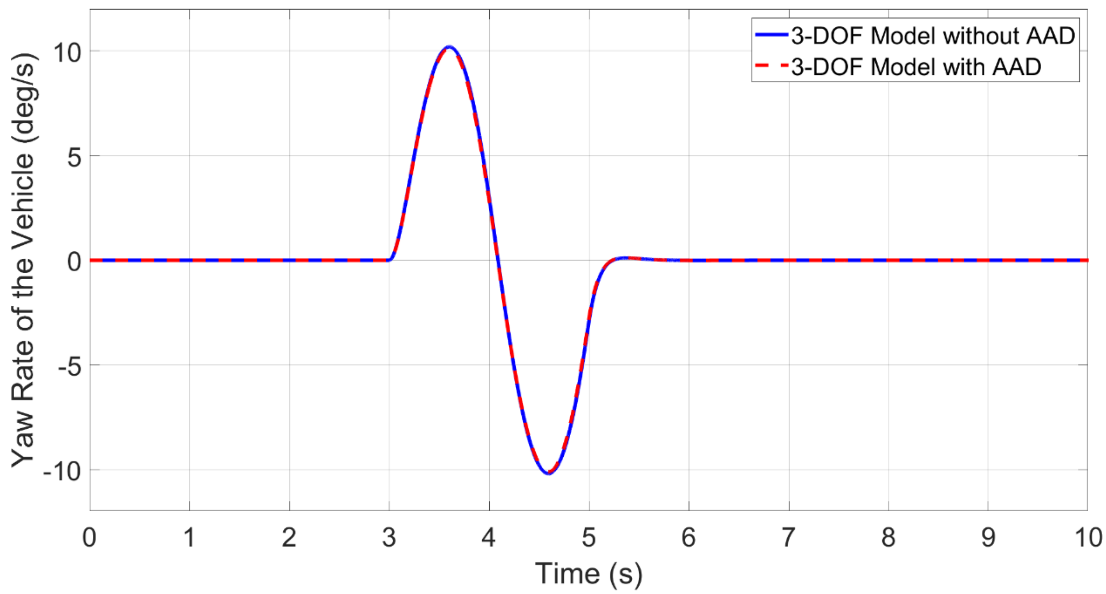

Figure 4.9: Time history of the yaw rates of the vehicle with and without the AAD system at 80 km/h.

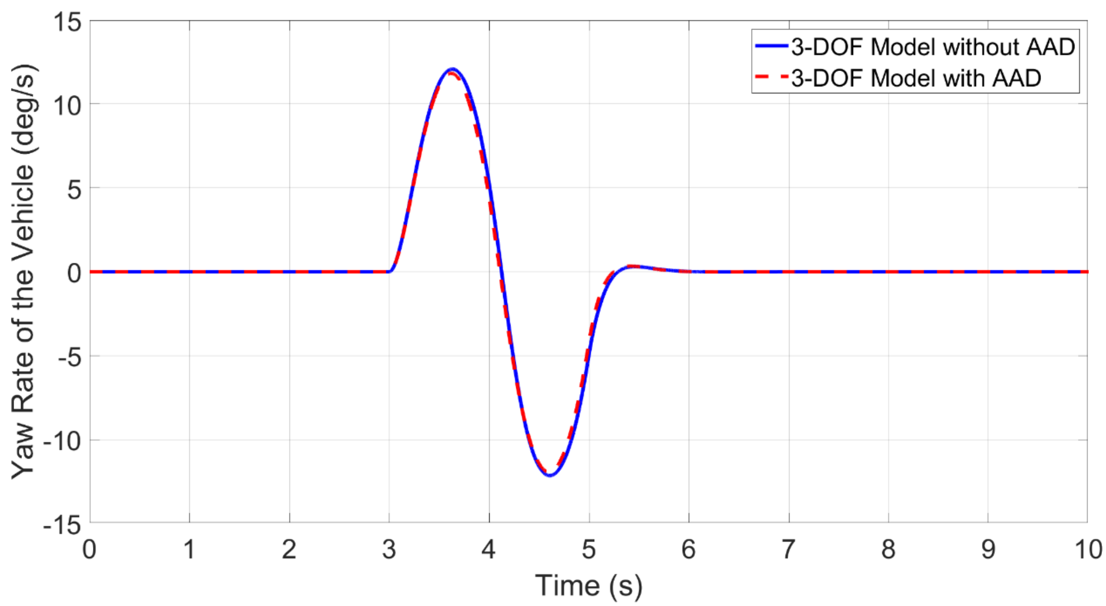

Figure 4.10: Time history of the yaw rates of the vehicle at with and without the AAD system at 100 km/h.

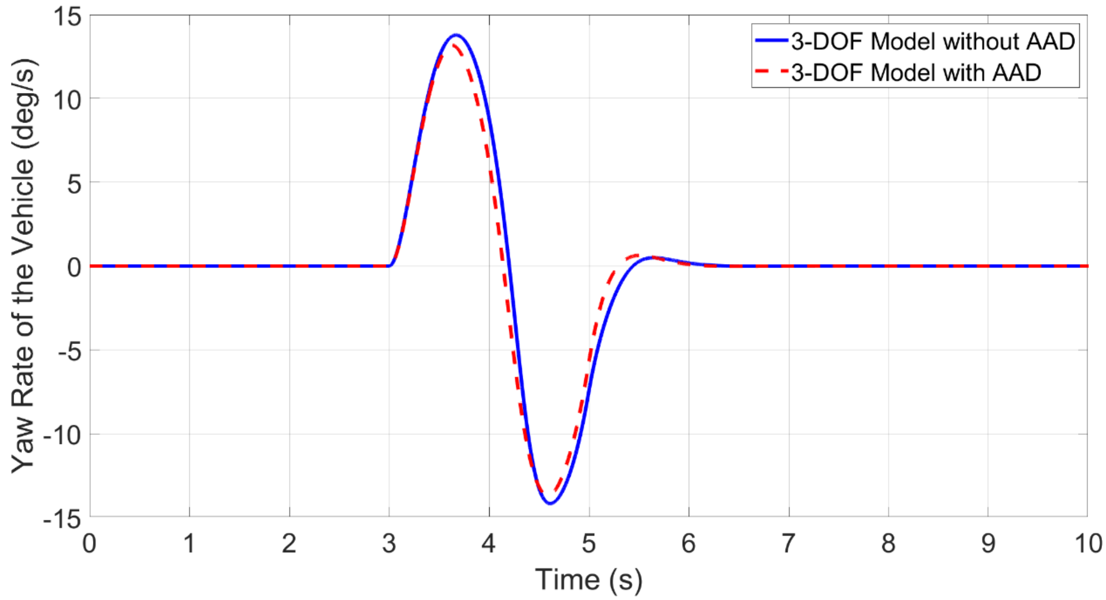

Figure 4.11: Time history of the yaw rates of the vehicle with and without the AAD system at 120 km/h.

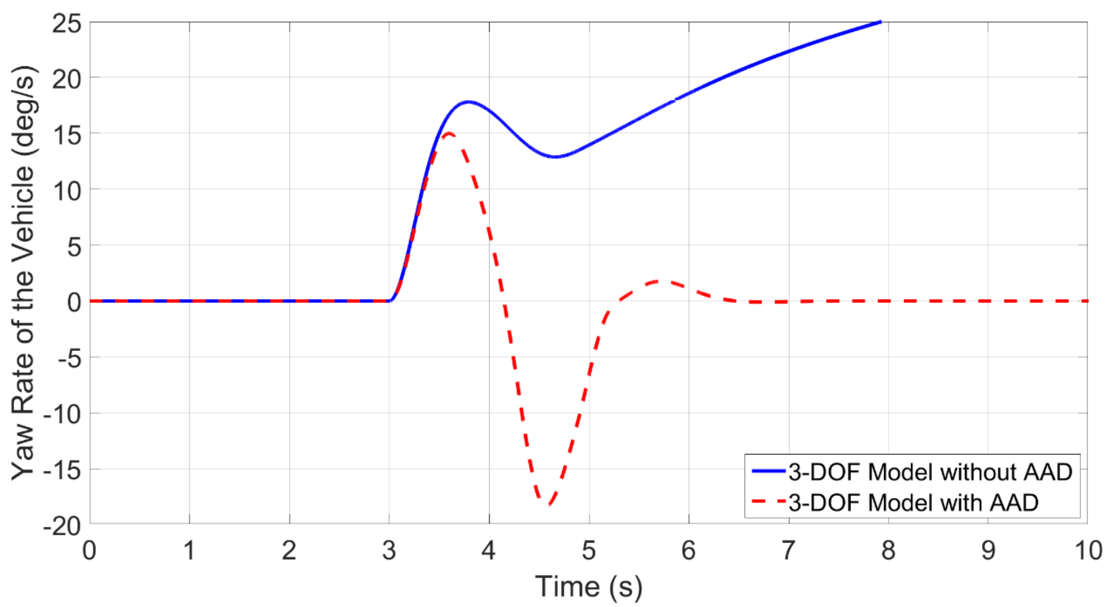

Figure 4.12: Time history of the yaw rates of the vehicle with and without the AAD system at 180 km/h.

Figure 4.13 illustrates the time history of the lateral displacements of the vehicle with and without AAD control at the speed of 180 km/h. Obviously, with the AAD controller, the vehicle will drift out laterally.

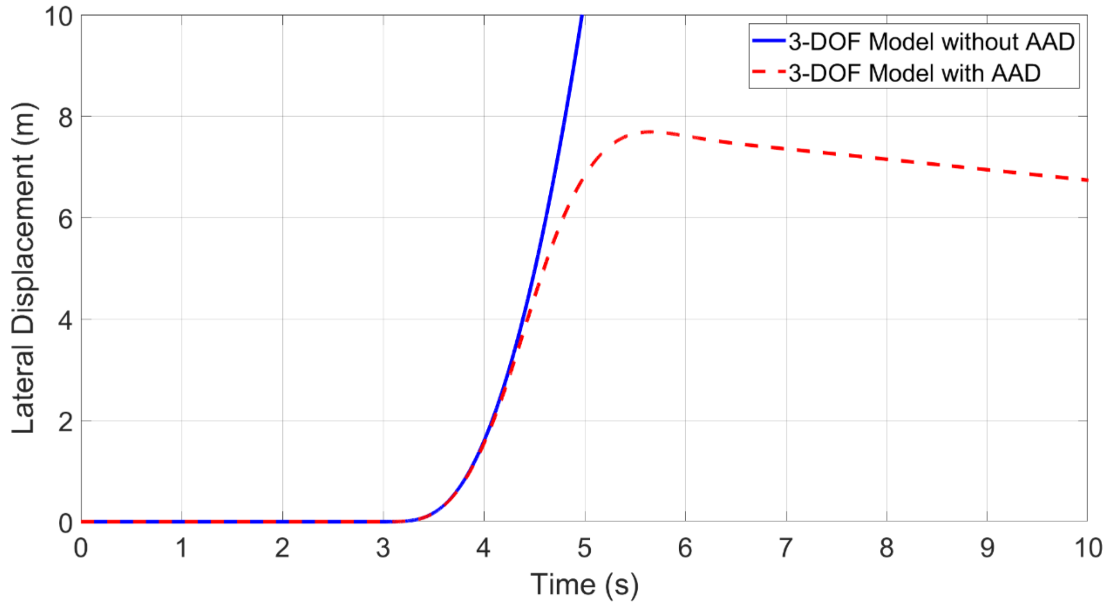

Figure 4.13: Time history of the lateral displacements of the vehicle with and without the AAD system at 180 km/h.

Figure 4.14 shows the improvement in performance over speed. It is demonstrated that the SMC controller can improve the yaw stability of the vehicle, especially, at high speeds.

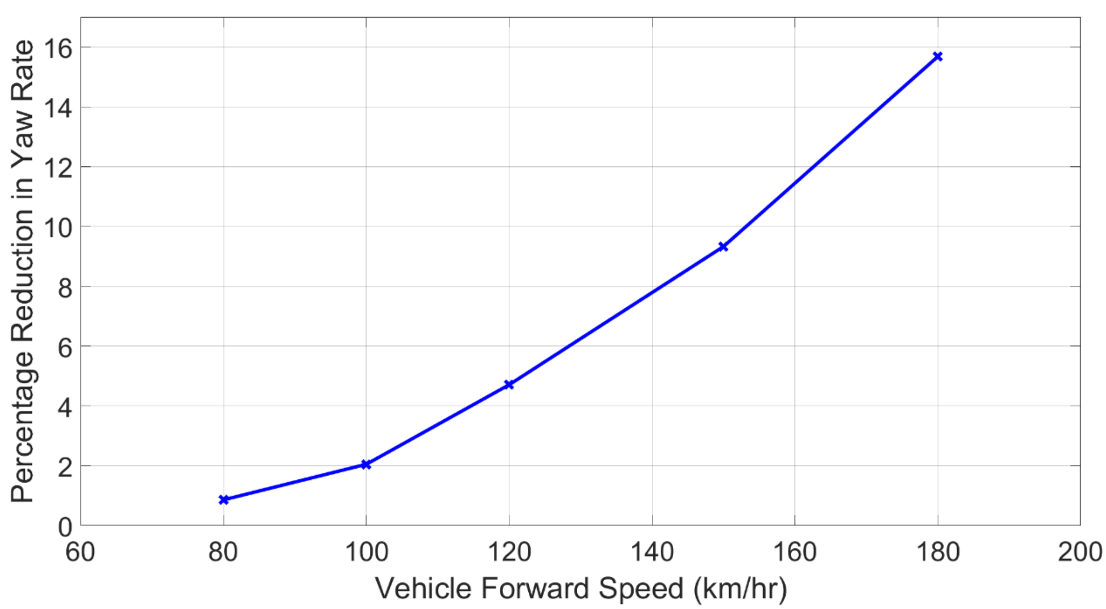

Figure 4.14: Improvement in performance of the AAD controller as speed increases.

4.3.4 Effect of Payload Variation (Robustness Test)

Robustness is a key characteristic of the proposed SMC controller along with its applicability to nonlinear systems. This feature is demonstrated in Figure 4.15, showing the relation between the peak yaw rate of the vehicle with and without AAD control and the variation of vehicle payload.

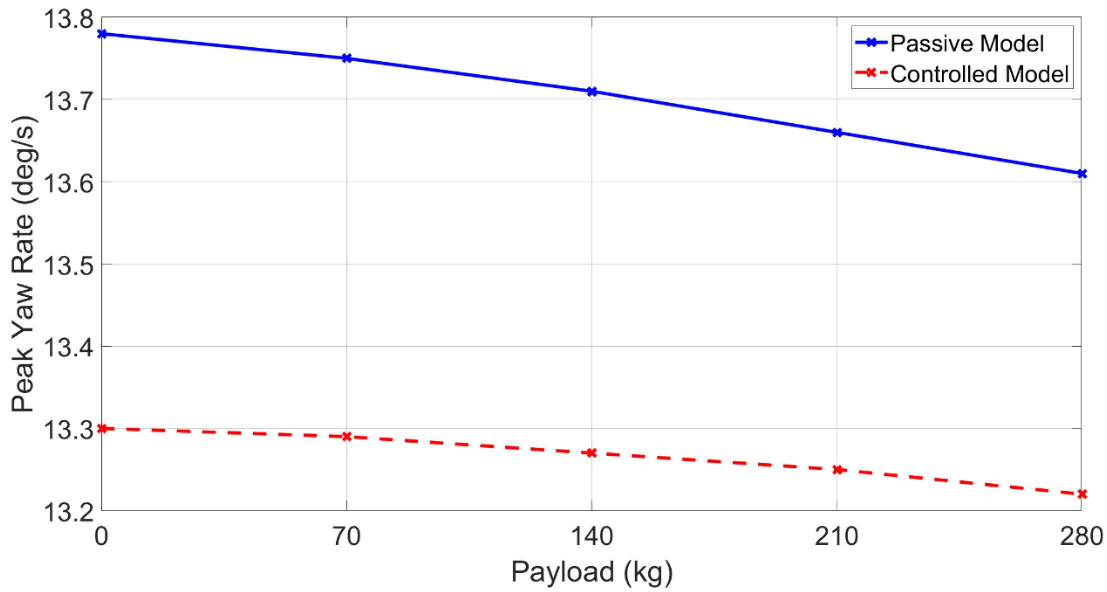

Figure 4.15: Variation of the peak yaw rates with an increase in payload.

As shown in Figure 4.15, the robustness of the AAD controller is checked by testing the vehicle at a constant speed of 120 km/h and changing the payloads while keeping the control parameters constant. It can be seen that the change of peak yaw rate with increasing payload is more for the passive vehicle as compared to the controlled vehicle. Thus, the control system is insensitive to payload variation. Additionally, the variation in the performance as the payload is changed can also be taken as a sufficient condition of robustness if the variation is less than 10% as shown in Table 4.2.

Table 4.2: Variation of the controller performance with varying payloads.

Payload (kg)	Percentage reduction in peak yaw rate i.e. performance measure	Percentage change in the performance measure
0	3.48	-
70	3.34	-4.02
140	3.21	-3.89
210	3	-6.54
280	2.86	-4.67

The second column in the above table contains values of the percentage reduction in peak yaw rate as a performance measure for each case where each case pertains to a different payload on the vehicle. As calculated in the third column, the change in the magnitude of the performance measure for all successive cases is less than 10%.

4.4 Summary

The design of the control system is the essence of this research. A controller design includes two main components, the control objective, and the control technique. Tracking a reference yaw rate is selected as the objective because of its comprehensiveness. The reference yaw rate is derived from the dynamics of a 2-DOF linear yaw plane model (i.e., the bicycle model), thereby forcing the vehicle to a linear range of dynamics to make it stable and controllable. The technique used is an improvised version of the SMC method that makes the controller independent of all the complex dynamical equations. The sliding mode control is aided with two external governing equations to define and characterize the control input as encapsulated in Figure 4.16.

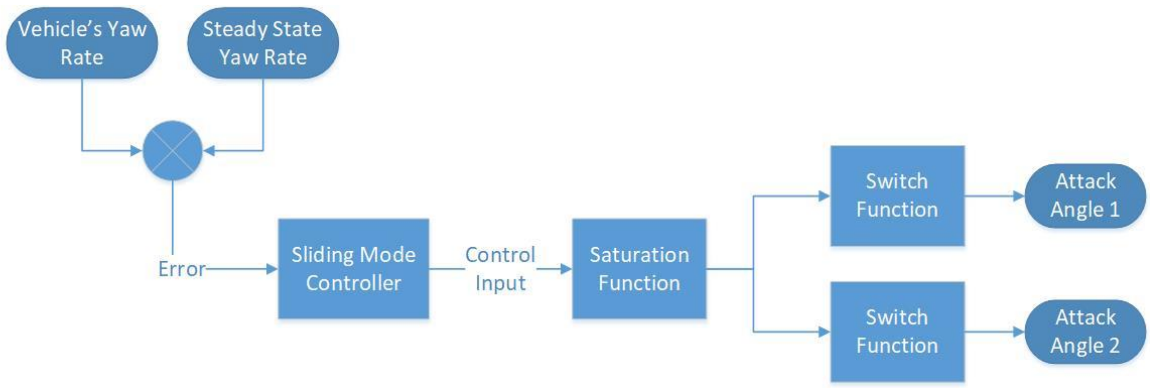

Figure 4.16: Block diagram of the active aerodynamic controller consisting of a sliding mode controller and other governing equations.

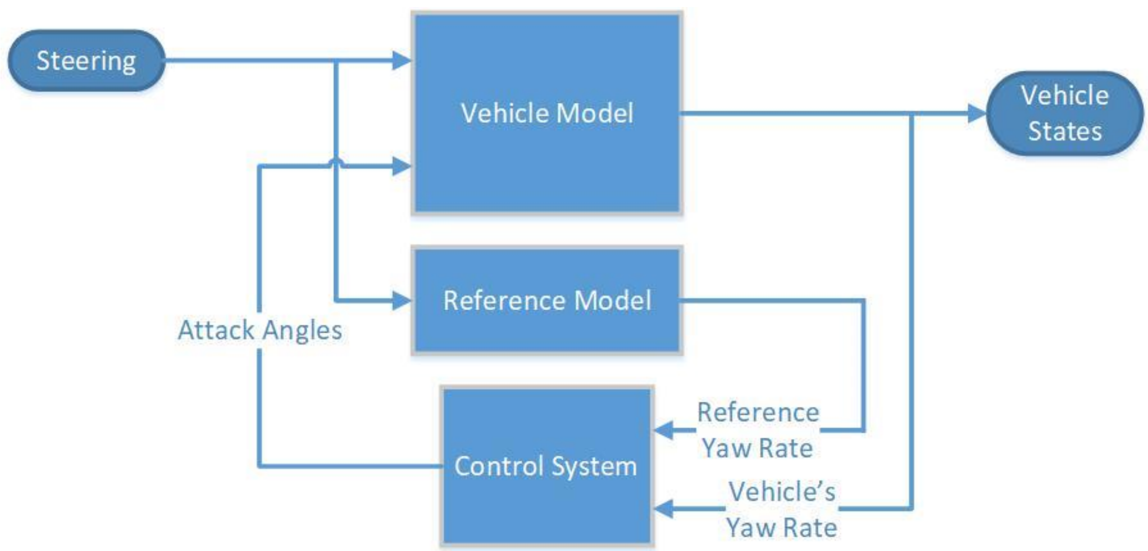

Figure 4.17: Block diagram of the Active Aerodynamic Control System.

Last of all, the working of the controller is shown by numerical simulations in MATLAB/Simulink. The interaction of the controller and the vehicle models in the Simulink software environment is shown in Figure 4.17.

Chapter 5

Validation of SMC-based AAD Controller using Co-Simulations

The proposed SMC-based AAD controller is validated using the co-simulations conducted in CarSim-MATLAB/Simulink environment. To this end, the SMC-based AAD controller designed in MATLAB/Simulink is integrated with the nonlinear 14-DOF vehicle model developed in CarSim using an interface, called S-Function. The co-simulations are conducted under four testing maneuvers: 1) step steer input, 2) fishhook, 3) double lane-change on a regular road surface, and 4) double lane-change on a slippery road surface. The first and second testing maneuvers belong to open-loop dynamic tests, while the third and fourth maneuvers are closed-loop dynamic tests. Under the third testing maneuver, the built-in driver model offered in CarSim drives the virtual vehicle (i.e., the 14-DOF nonlinear vehicle model) with the AAD controller tracking a predefined yaw rate for a given forward speed and front wheel steering angle.

5.1 Step Steer Input

The first test is a step steer maneuver. It is like a racing car cornering maneuver. Figure 5.1 shows the time history of the front wheel steer angle. Over the testing maneuver, the vehicle travels at the forward speed of 150 km/h.

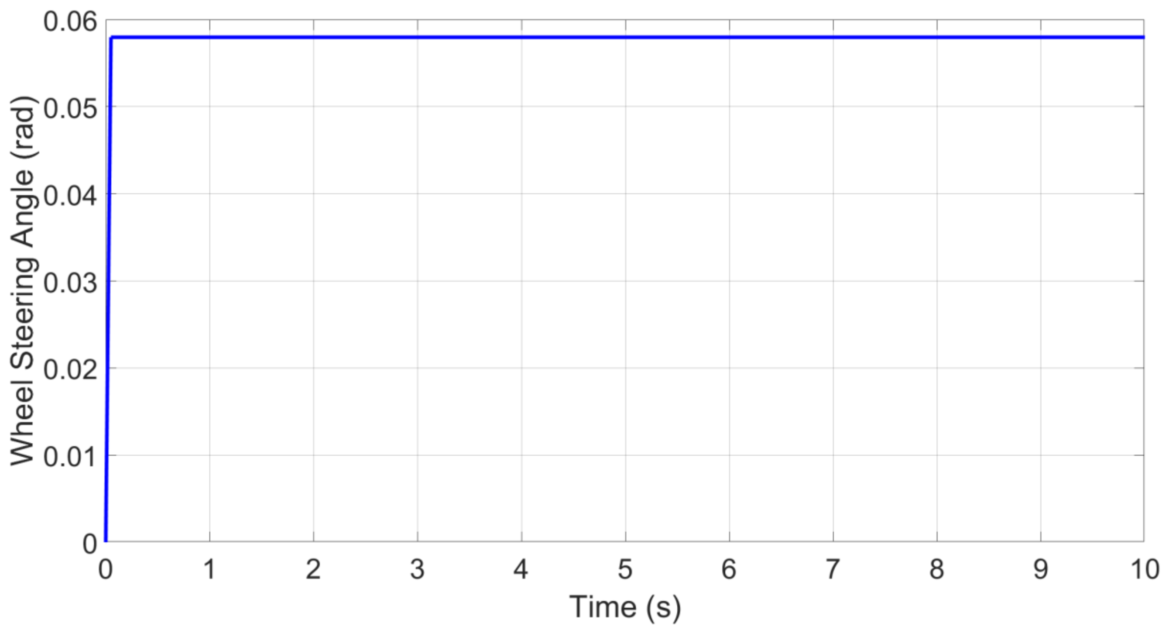

Figure 5.1: Time history of the step steer input of the front wheel.

Figures 5.2, 5.3, and 5.4 show the simulation results in terms of the time history of yaw rate, sideslip angle, and lateral acceleration, respectively. It is shown that the oscillations of the yaw rate, the sideslip angle, and the lateral acceleration of the controlled vehicle are damped with lesser peak values and settling time, compared against those of the uncontrolled vehicle.

Figure 5.5 demonstrates the effect of the control action on the downforces. To improve the yaw stability, the controller increases the load of the outer wheel by lifting the outer wing. Although the static downforces due to the base position of the wings adversely affect the control objective, this effect is satisfactorily compensated by the controller as it produces the difference in the downforces acting on the two tires.

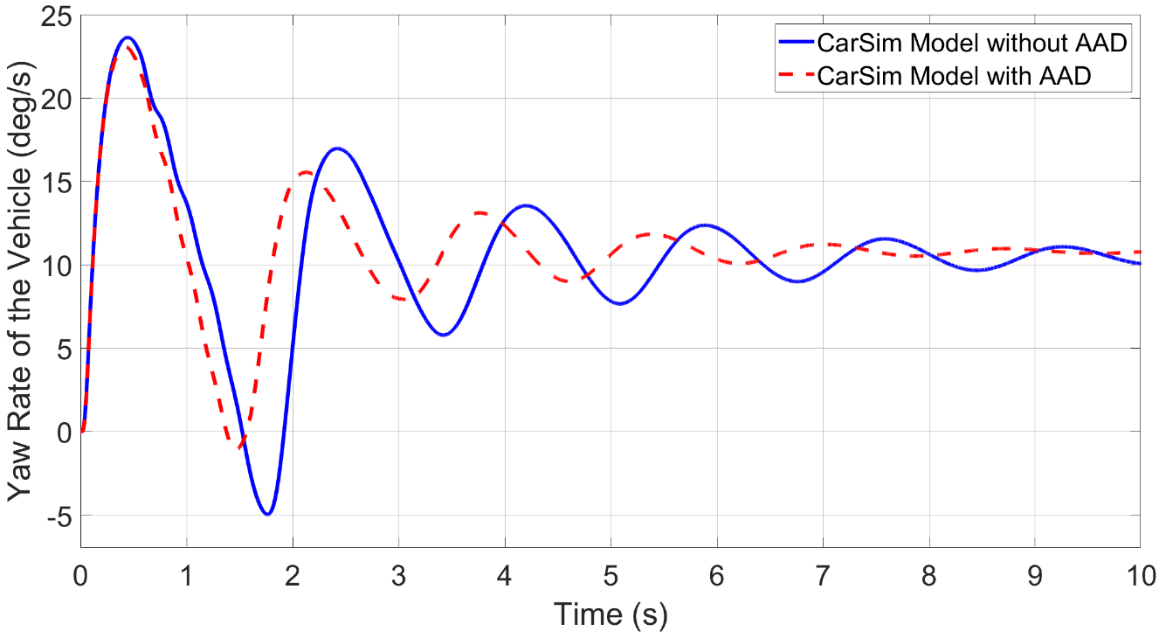

Figure 5.2: Time history of the yaw rate of the vehicle with and without the AAD system under the step steer maneuver at the forward speed of 150 km/h.

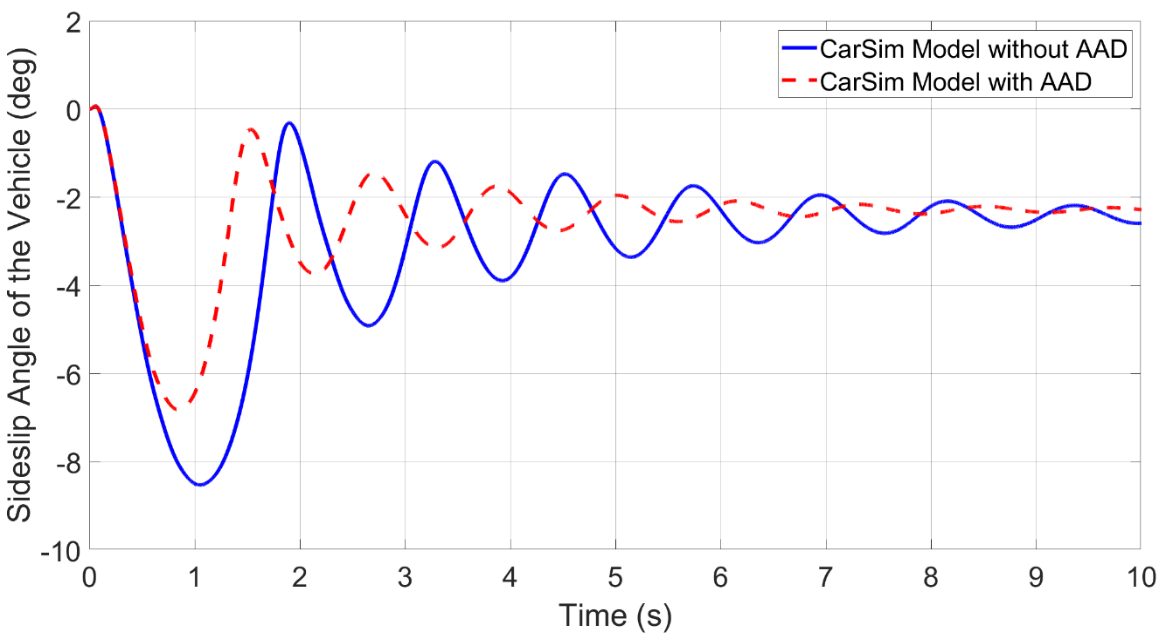

Figure 5.3: Time history of the sideslip angle of the vehicle with and without the AAD system under the step steer maneuver at the forward speed of 150 km/h.

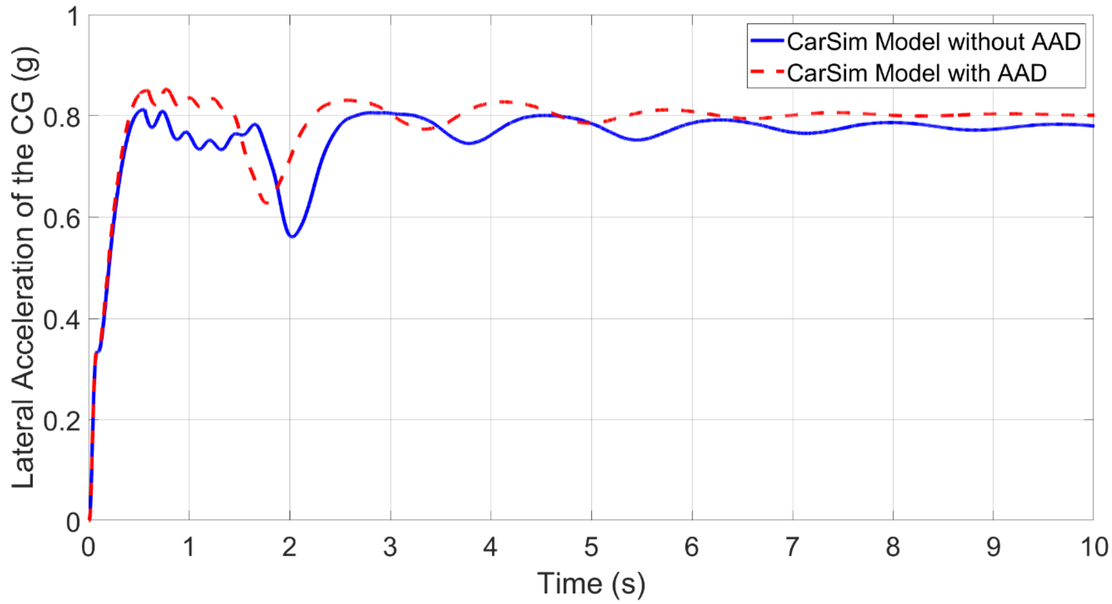

Figure 5.4: Time history of the lateral acceleration of the vehicle with and without the AAD system under the step steer maneuver at the forward speed of 150 km/h.

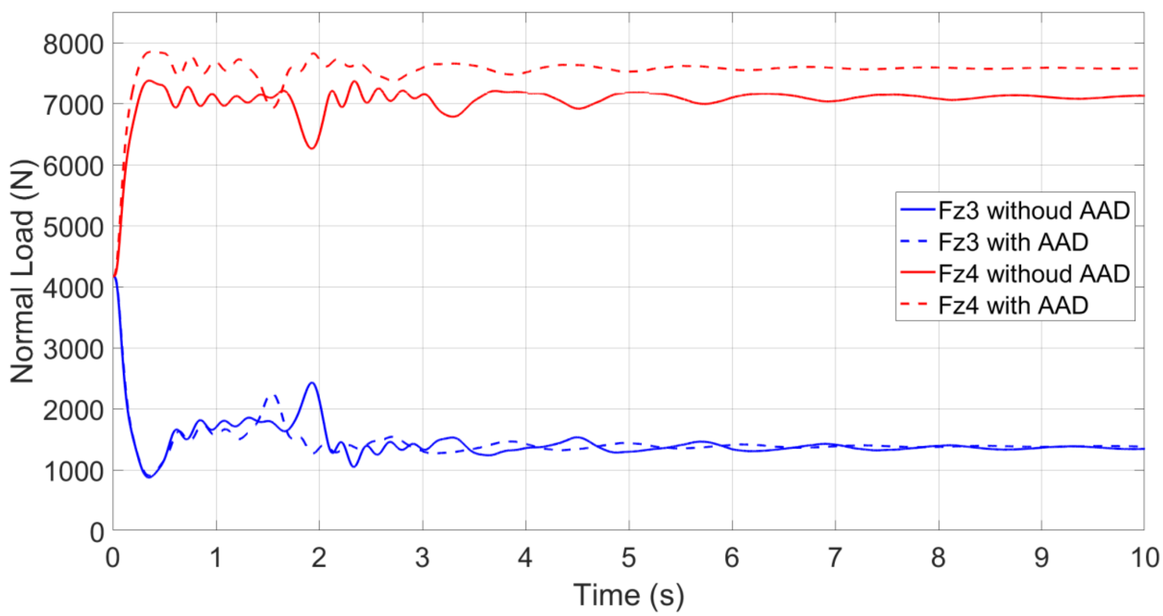

Figure 5.5: Time history of the normal loads acting on the rear tires of the vehicle with and without the AAD system under the step steer maneuver at the forward speed of 150 km/h.

Figure 5.6 illustrates the paths of the vehicle with and without the AAD controller. It is evident that the controlled vehicle travels along a circle with a shorter radius than the baseline vehicle. The simulation result shown in Figure 5.6 indicates that the AAD controller improves the maneuverability of the vehicle.

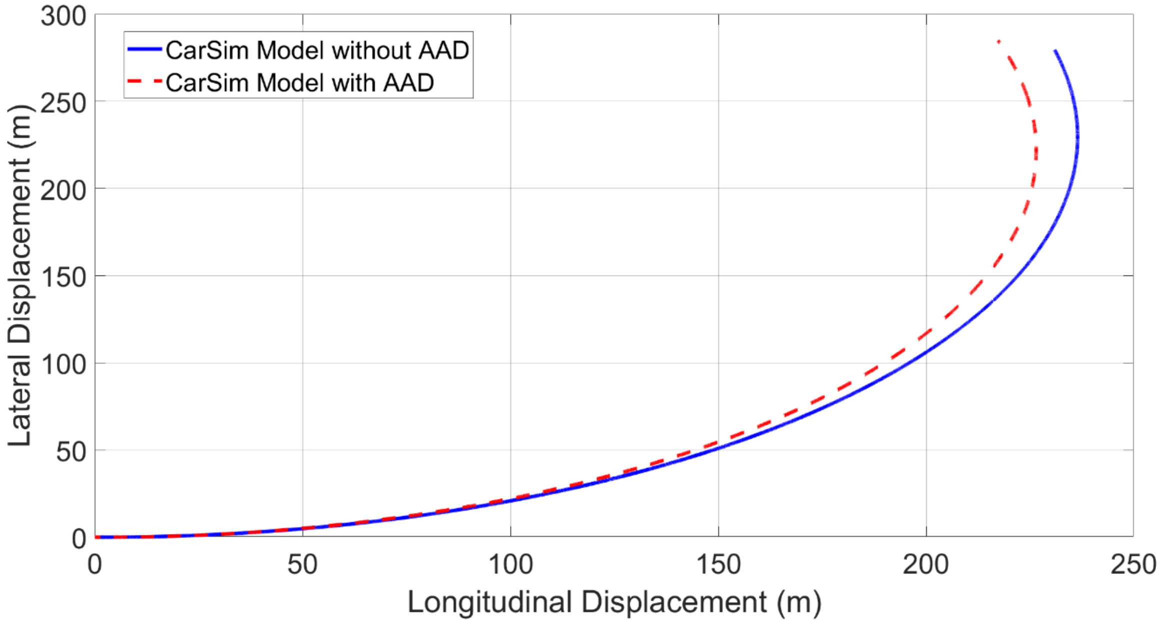

Figure 5.6: Paths of the vehicle with and without the AAD system under the step steer maneuver at the forward speed of 150 km/h.

5.2 Fishhook

The fishhook test is a rapid turning maneuver with high magnitudes of the steering angle. By means of simulating the severe testing maneuver, the vehicle's stability measures may be evaluated. Figure 5.7 shows the time history of the steering angle of the front wheels.

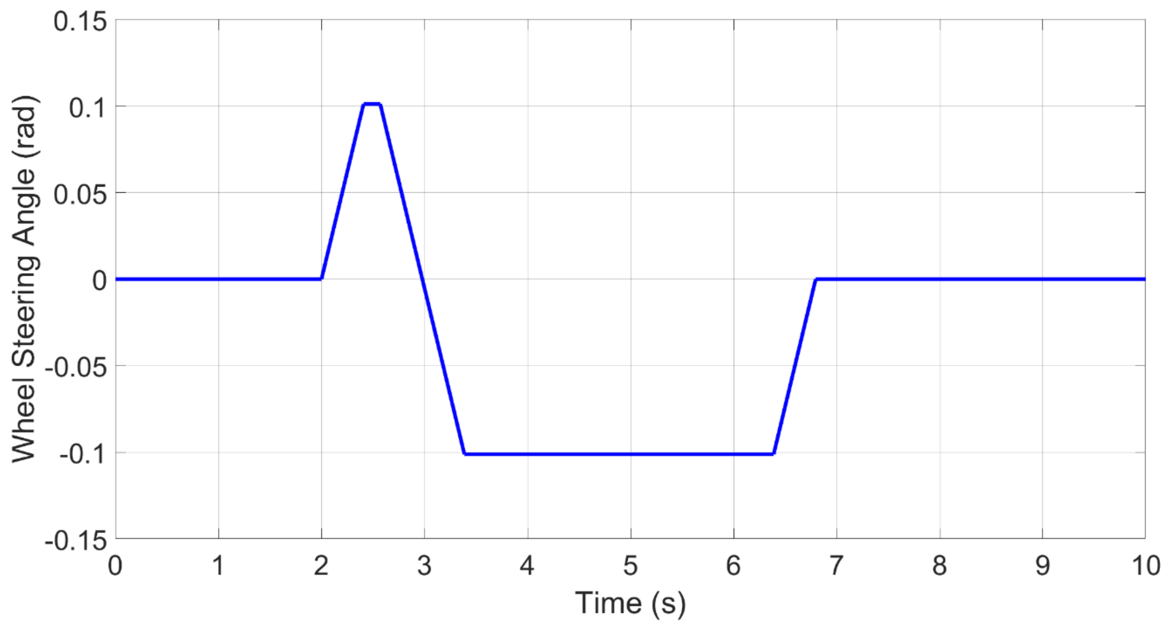

Figure 5.7: Time history of the front wheel steering input.

The test is conducted at various speeds. The results of the test speed at which the uncontrolled model spins out are presented. Figures 5.8 and 5.9 present the time history of the yaw rate and the sideslip angle as the vehicle undergoes the fishhook steer input testing maneuver at the forward speed of 150 km/h. Both of the states of the controlled model are shown to return to a steady state, while the passive model loses the yaw stability. Figure 5.10 demonstrates the spinning out of the uncontrolled vehicle near the end of the maneuver. The spin-out occurs as the tires lose traction with the ground because of the intense steering action. In the case of the controlled vehicle, the wings produce additional downforces and enhance the road holding capability of the tires.

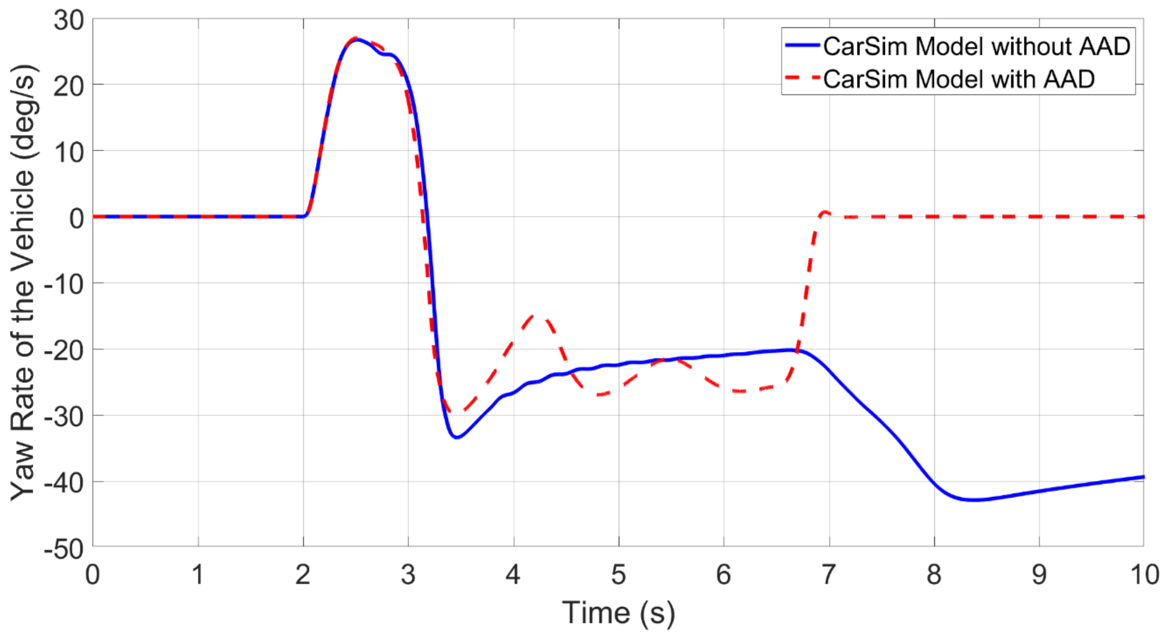

Figure 5.8: Time history of the yaw rate of the vehicle with and without the AAD system under the fishhook maneuver at the forward speed of 150 km/h.

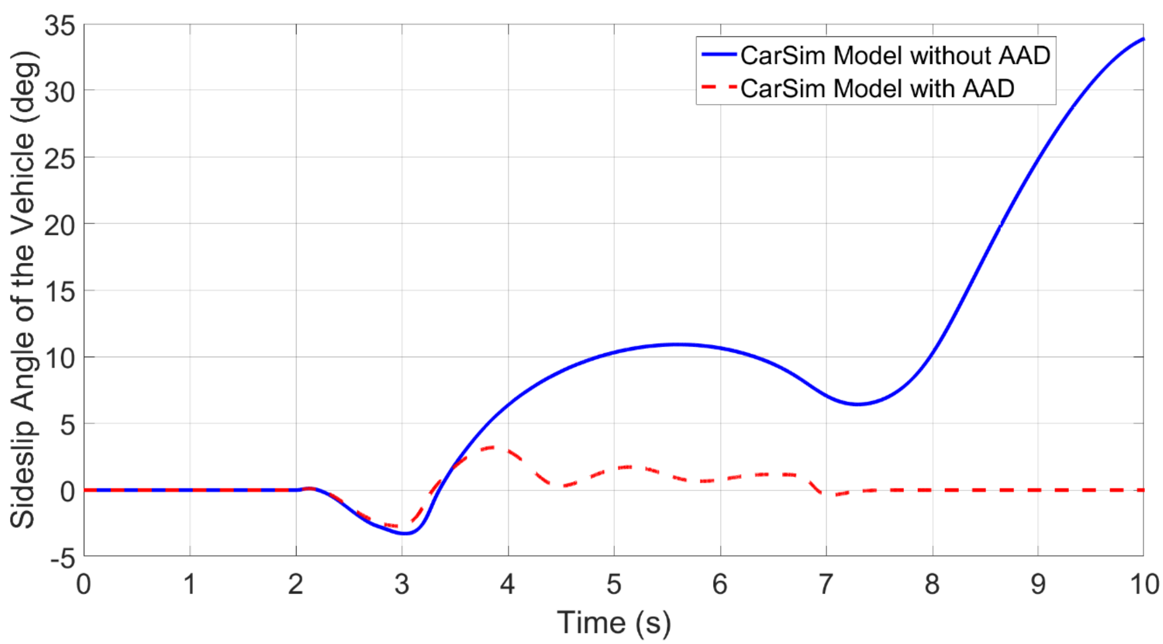

Figure 5.9: Time history of the sideslip angle of the vehicle with and without the AAD system under the fishhook maneuver at the forward speed of 150 km/h.

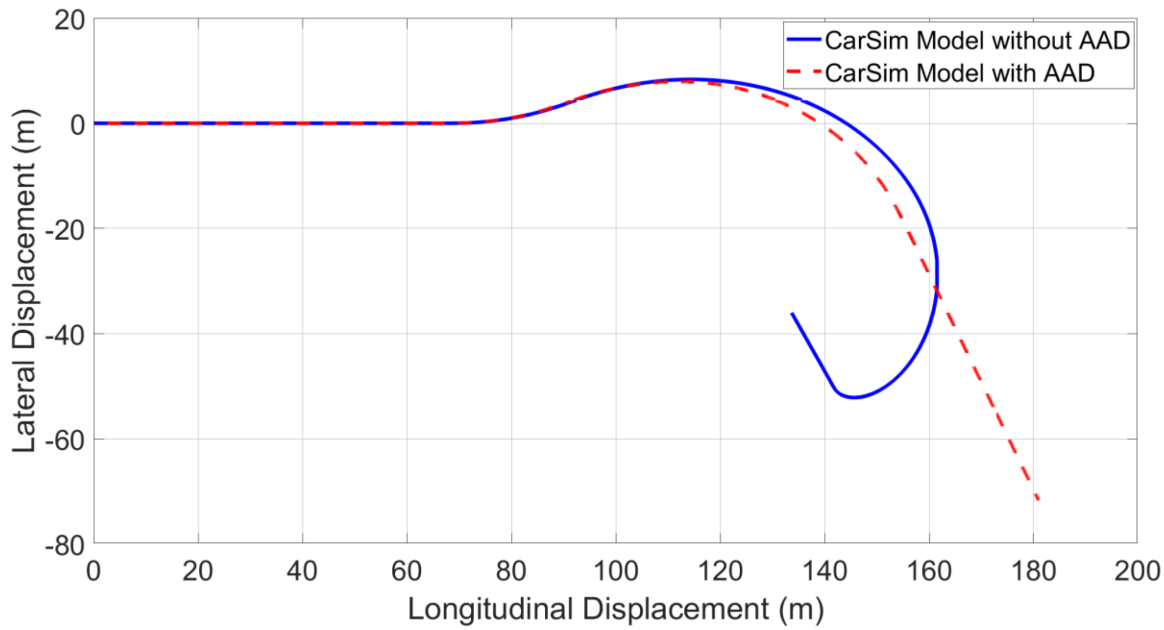

Figure 5.10: Path of the vehicle with and without the AAD system under the fishhook maneuver at the forward speed of 150 km/h.

5.3 Double Lane Change on Regular Road Surface

This section further validates the controller by simulating the double lane change maneuver on a regular road surface with a friction coefficient of 0.85 between the tire and road surface. Figures 5.11 and 5.12 illustrate the simulation results in terms of the time history of yaw rate and sideslip angle of the vehicle with and without the AAD controller under the double lane change maneuver at the forward speed of 150 km/h. It is observed that the controller improves the yaw stability of the vehicle by reducing the peak values of the yaw rate and sideslip angle over the testing maneuver. Figure 5.13 shows the trajectories of the vehicle with and without the AAD controller under the simulated double lane change maneuver at 150 km/h. It is disclosed that the controller imposes a minor impact on the path-following capability under the maneuver at the speed of 150 km/h.

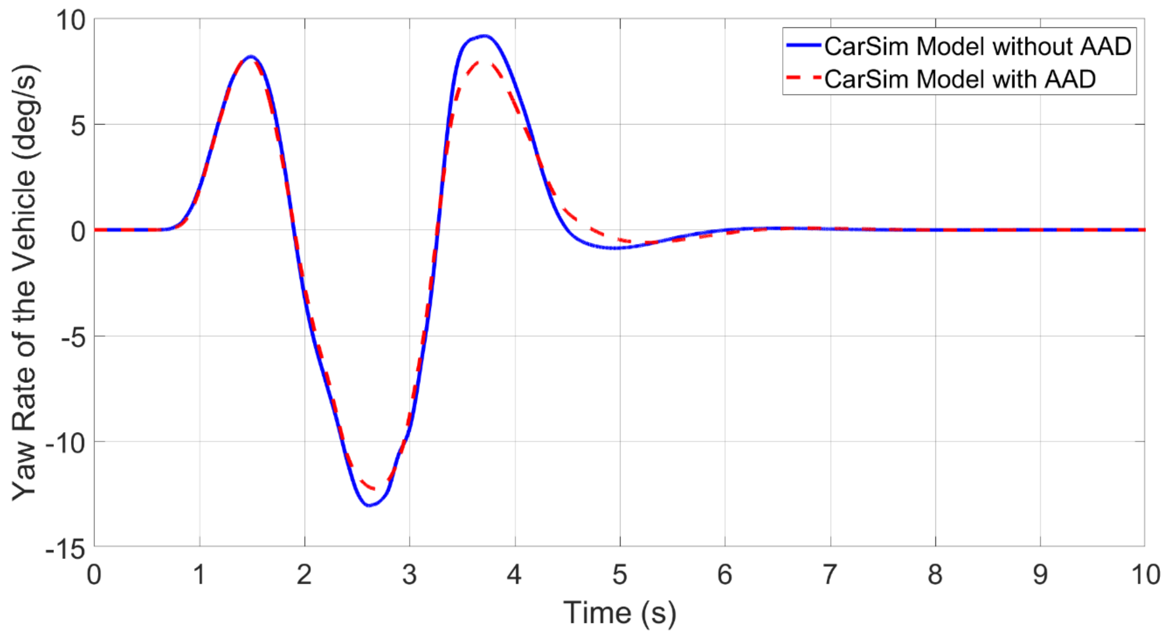

Figure 5.11: Time history of the yaw rate of the vehicle due to a double lane change maneuver, with and without the AAD system, at 150 km/h.

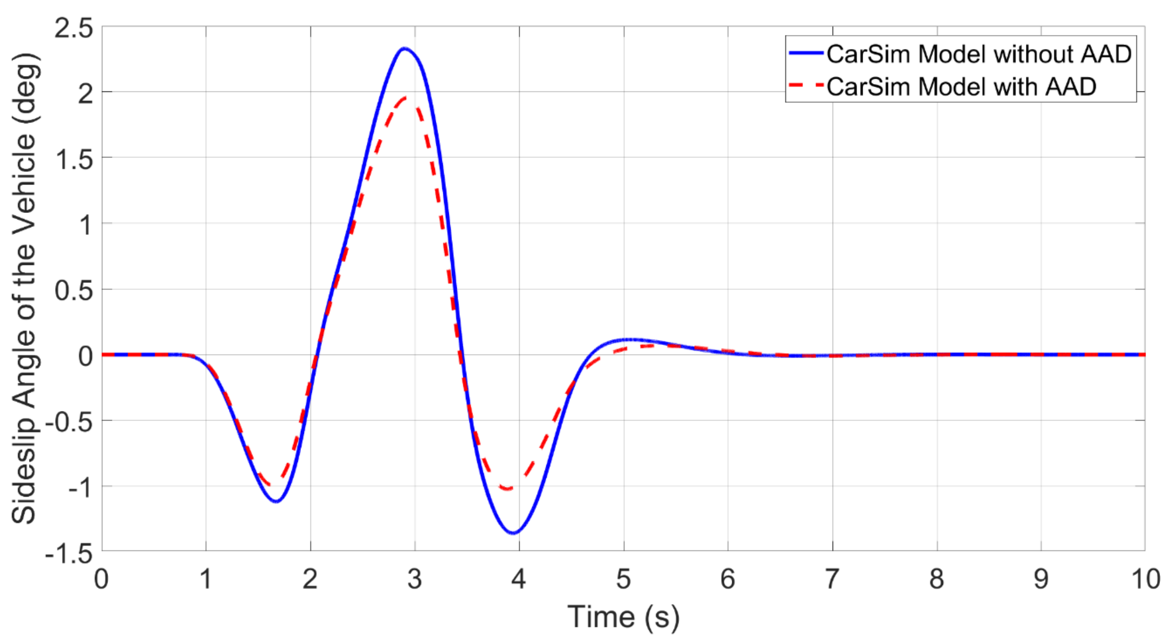

Figure 5.12: Time history of the sideslip angle of the vehicle due to a double lane change maneuver, with and without the AAD system, at 150 km/h.

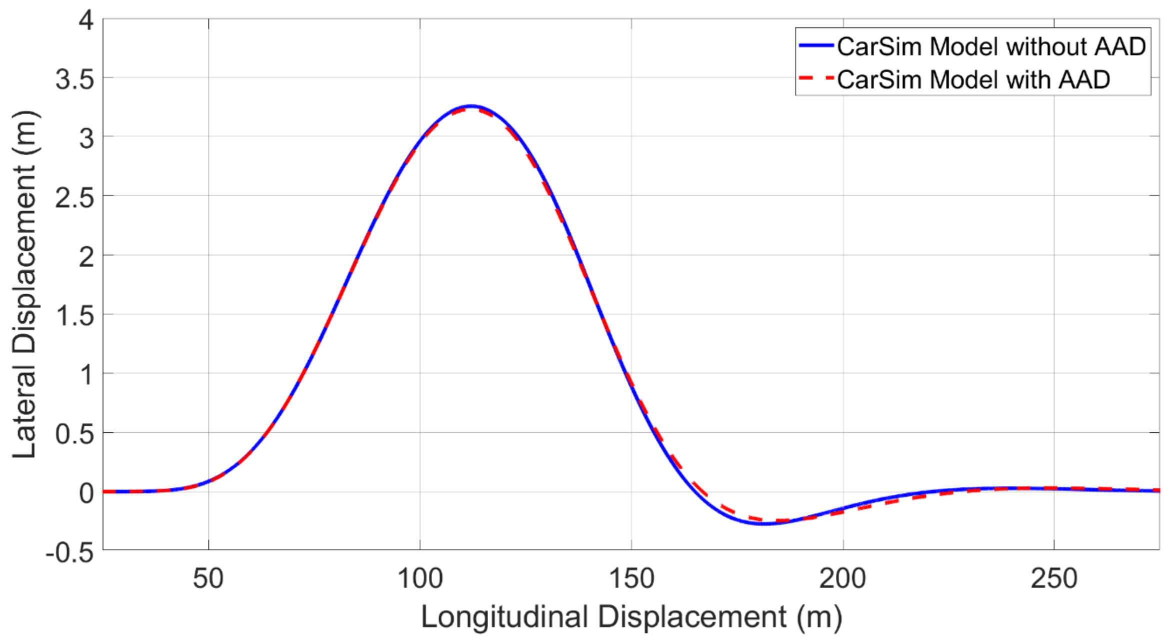

Figure 5.13: Path followed by the vehicle due to a double lane change maneuver, with and without the AAD system, at 150 km/h.

Figures 5.14 and 5.15 show the simulation results in terms of the time history of yaw rate and sideslip angle of the vehicle with and without the AAD controller under the double lane change maneuver at the forward speed of 200 km/h. Compared with the respective simulation results shown in Figures 5.11 and 5.12 at the forward speed of 150 km/h, the results shown in Figures 5.14 and 5.15 indicate that the controller is more effective for improving the yaw stability of the vehicle in terms of yaw rate and sideslip angle at higher speeds. Figure 5.16 shows the trajectories of the vehicle with and without the AAD controller under the double lane change maneuver at the forward speed of 200 km/h. Interestingly, at the high speed, the controller can also improve the path-following ability of the vehicle.

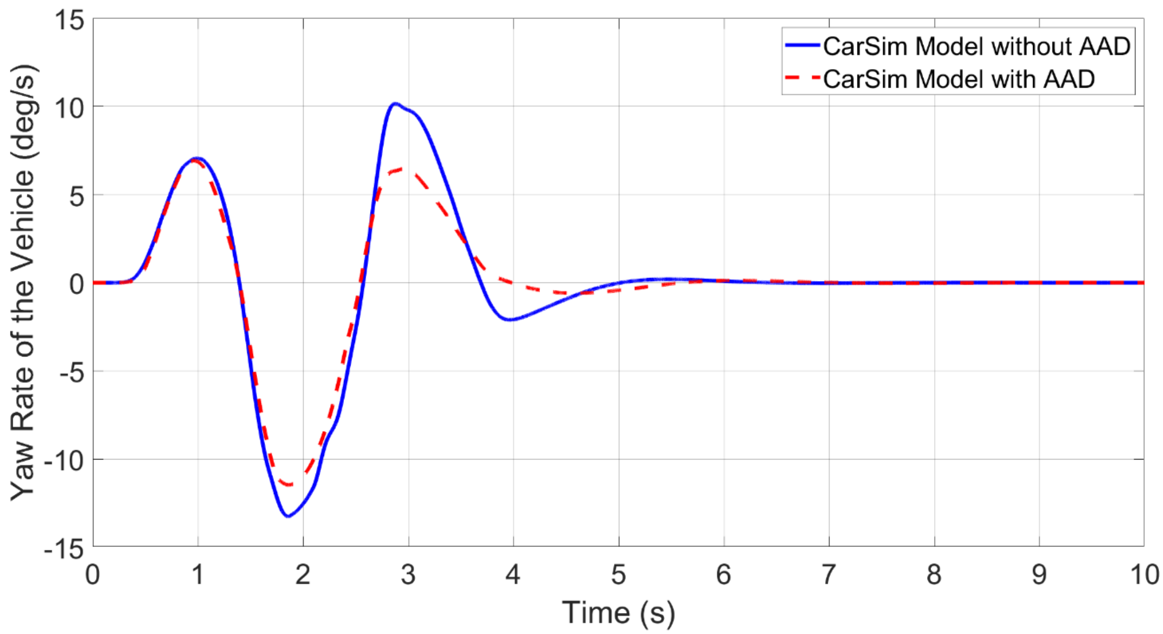

Figure 5.14: Time history of the yaw rate of the vehicle with and without the AAD system under the double lane change maneuver at the forward speed of 200 km/h.

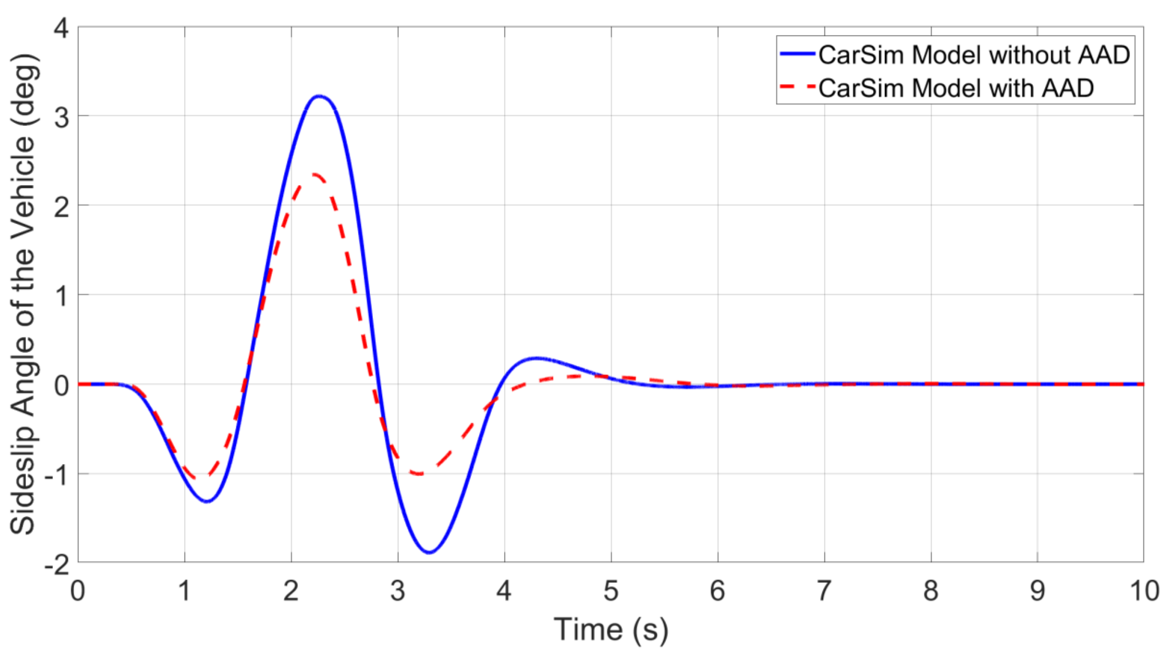

Figure 5.15: Time history of the sideslip angle of the vehicle with and without the AAD system under the double lane change maneuver at the forward speed of 200 km/h.

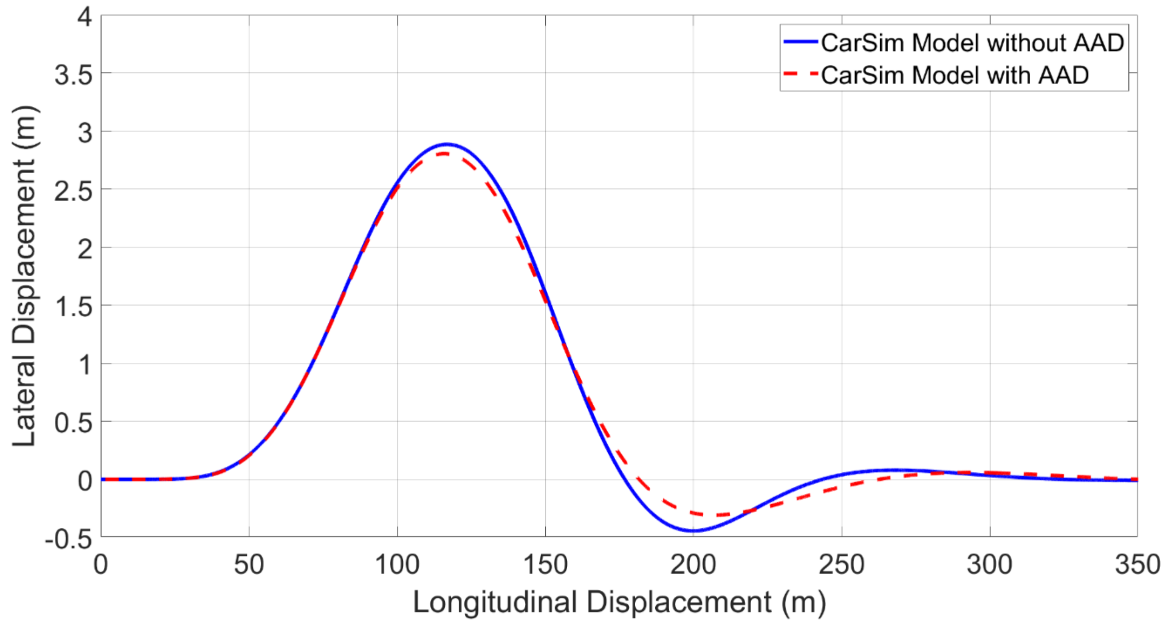

Figure 5.16: Paths of the vehicle with and without the AAD system under the double lane change maneuver at the forward speed of 200 km/h.

5.4 Double Lane Change on Slippery Road Surface

The final test is a double lane change on a low friction road surface with a friction coefficient of 0.5 between the tires and the road surface. Figures 5.17, 5.18, and 5.19 show the simulation results of the vehicle with and without the AAD controller under the double lane change maneuver on the slippery road surface at the forward speed of 84 km/h. The results are shown in terms of the dynamic responses of yaw rate, sideslip angle, and trajectory of the vehicle over the maneuver. Simulation results reveal that on the slippery road surface, the baseline vehicle loses the yaw stability even at the forward speed of 84 km/h. In contrast, with the proposed AAD controller, the vehicle can successfully execute the double lane change maneuver on the slippery road surface. Figure 5.20 exhibits a snapshot of the vehicle with and without the AAD controller at the end of the double lane change maneuver on the slippery road surface. Obviously, the baseline vehicle loses its yaw stability, while the vehicle with the AAD controller is able to along the predefined path.

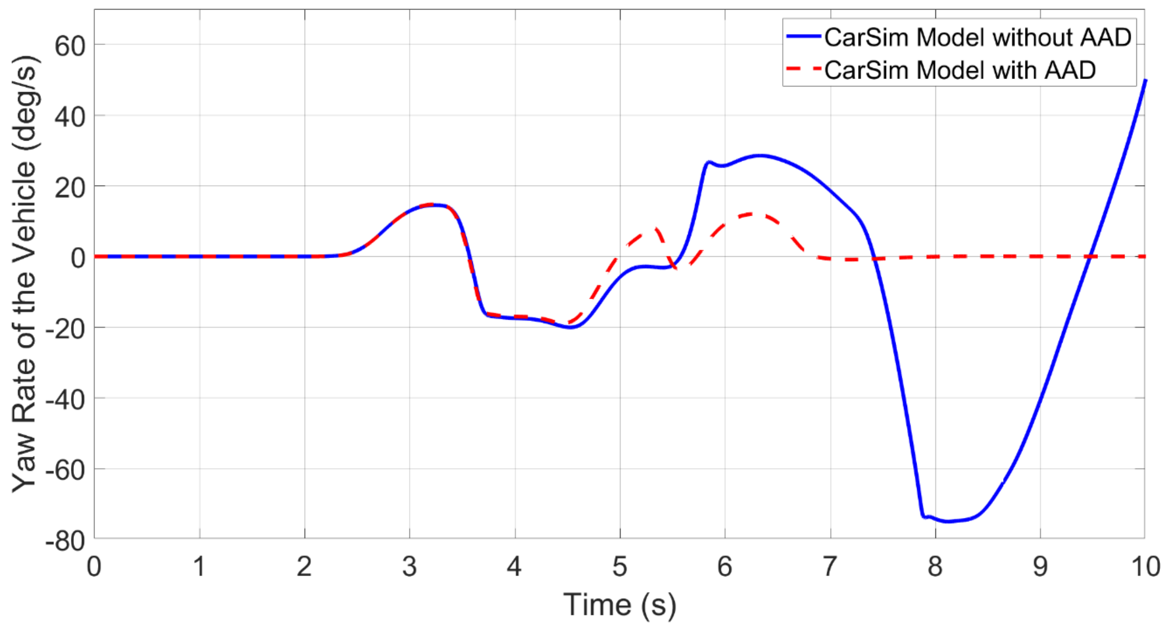

Figure 5.17: Time history of the yaw rate of the vehicle with and without the AAD system under the double lane change maneuver on a slippery surface at the forward speed of 84 km/h.

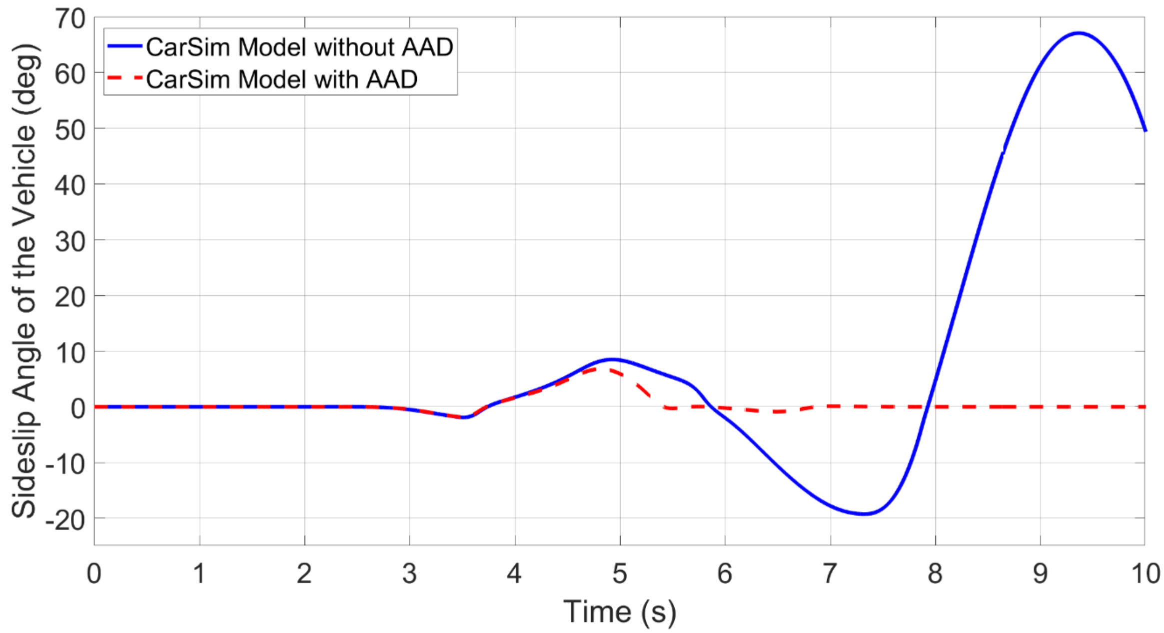

Figure 5.18: Time history of the sideslip angle of the vehicle with and without the AAD system under the double lane change maneuver on a slippery surface at the forward speed of 84 km/h.

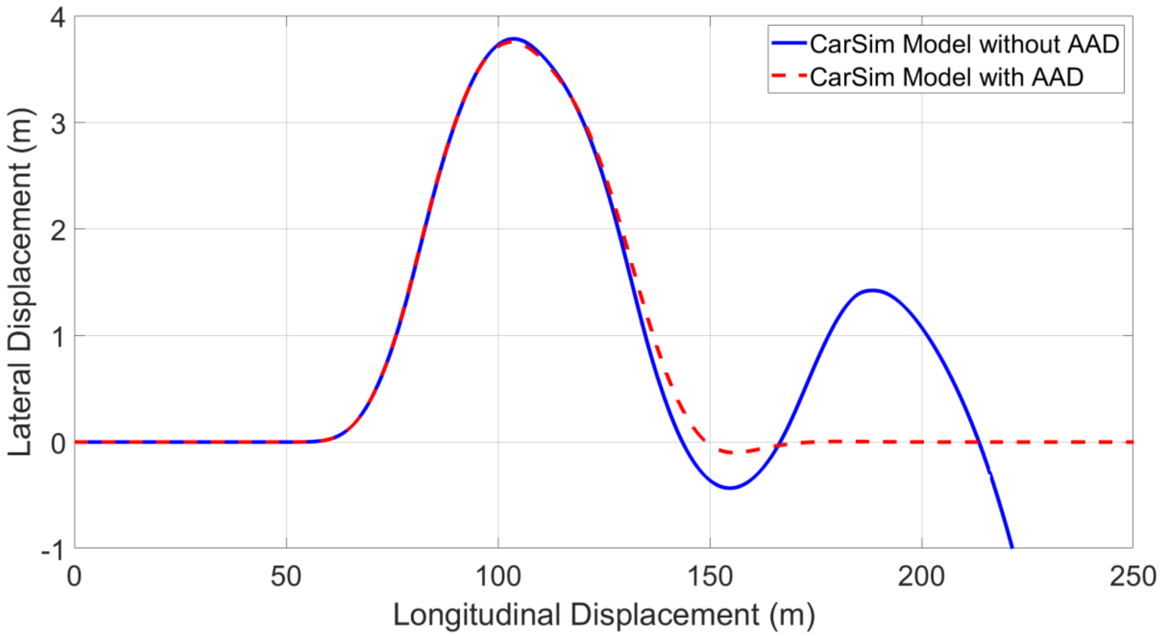

Figure 5.19: Paths of the vehicle with and without the AAD system under the double lane change maneuver on a slippery surface at the forward speed of 84 km/h.

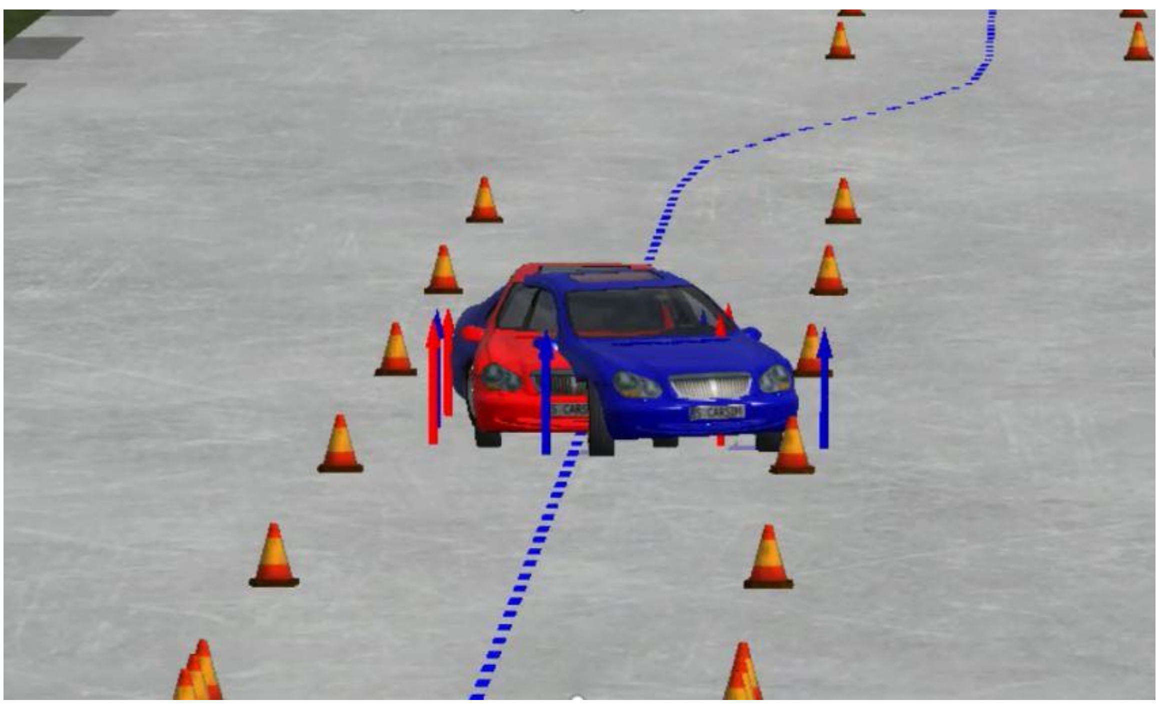

Figure 5.20: A snapshot of the two vehicles (red: controlled; blue: passive)) at the end of the double lane change maneuver on a slippery surface at the forward speed of 84 km/h.

5.5 Summary

The proposed SMC-based AAD controller has been validated using the co-simulations conducted in the CarSim-MATLAB/Simulink environment. To adequately evaluate the performance of the AAD controller, both open- and closed-loop dynamic simulations are conducted. Simulation results reveal the following insightful findings:

1) The AAD controller can improve both the yaw stability and path-following capability of the vehicle under evasive maneuvers at high speeds.
2) The higher the forward speed, the more effective the AAD controller shows its performance.
3) The AAD controller demonstrates its superior performance in improving the lateral stability and enhancing the path-following capability under evasive maneuvers on slippery road surfaces.

Chapter 6

Conclusions

6.1 Conclusions

The safety of high-speed road vehicles is compromised under tight cornering maneuvers or over slippery surfaces. To increase the safety, the forces/torques generated due to the interactions of tires and road surface must be complemented with additional forces/torques. In this regard, to date, the application of aerodynamic forces/torques has not received much attention. Therefore, an active aerodynamic (AAD) system is proposed to increase the safety of high-speed road vehicles. The AAD system consists of two movable rear wings controlled by an SMC-based controller. The proposed AAD system has been tested, evaluated and validated using numerical simulations.

To develop the SMC-based AAD controller, a 2-DOF linear yaw-plane (bicycle) model is used to derive the steady-state yaw rate. The steady-state yaw rate is set as a reference for the controller to follow. A 3-DOF nonlinear yaw-roll model is derived to simulate the dynamics of the vehicle. The 3-DOF model facilitates the study of aerodynamic effects and proves to be a good trade-off between simplicity and accuracy. The controller is validated using a 14-DOF nonlinear model generated in the CarSim software package. The CarSim model is highly accurate as it has been authenticated by experimental and numerical results. A CAD model of the rear wings is created using the NX software package. The aerodynamic forces for the wings are obtained through the CFD simulations conducted using ANSYS Fluent software. The aerodynamic coefficients are then calculated using an appropriate formulation. One dimensional lookup tables are constructed in MATLAB/Simulink to integrate the aerodynamics and the vehicle dynamics.

An SMC technique is used to design the AAD controller to control the attack angles of the wings based on the decided control objective of tracking the steady-state yaw rate. Among three possible operating modes, the couple of the rear tires' tractive forces is selected based on the high lift to drag ratio of the wing model to generate the corrective yaw moment. The SMC-based controller design is simplified and supported with two governing equations to restrict the control action to physical limits. The 3-DOF model is simulated using the MATLAB/Simulink software package equipped with the AAD system. The performance of the controlled vehicle model is compared with that of the baseline vehicle without rear wings. The test is initialized with a single sinewave as steer input. Results show that the AAD system increases the safety of the vehicle. The important state variables are shown to be positively affected by the controller. Moreover, the variation in lateral load transfer due to the AAD system is also presented. It is demonstrated that the controller is more effective to improve the lateral stability of the vehicle at higher speeds. The analysis is concluded by simulating the vehicle with different payloads, thereby proving the controller's robustness.

The SMC-based AAD controller designed in MATLAB/Simulink is integrated with the 14-DOF nonlinear model developed in CarSim for co-simulations to validate the effectiveness of the controller. The dynamics of the vehicle with and without the AAD controller is simulated under a number of evasive maneuvers. The achieved dynamic responses of the vehicle with and without the AAD controller are compared and analyzed. The co-simulation results reveal the following insightful findings:

1) The AAD controller can improve both the yaw stability and path-following capability of the vehicle under evasive maneuvers at high speeds.
2) The higher the forward speed, the more effective the AAD controller shows its performance.
3) The AAD controller demonstrates its superior performance in improving the lateral stability and enhancing the path-following capability under evasive maneuvers on slippery road surfaces.

It can be concluded that this thesis will pave the way for extensive research on the implementation of active aerodynamic systems for high-speed road vehicles.

6.2 Recommendations for Future Studies

Built upon the innovative investigations of the research, the following recommendations are offered for future studies:

- Wing Design and Configuration: The size, shape, and placement of the wings is a crucial factor in active aerodynamic control. An in-depth analysis can be conducted by changing the position of the wings and/or by selecting different airfoil shapes for designing the wing. This may lead to a change in the selection of the operating mode. For example, if a wing is designed with a very low lift to drag ratio it may be worthwhile to implement the first operating mode.

- Multi-objective Control: Though the single objective control has proved to be a simple yet effective control strategy, there is the possibility of an improvement in vehicle performance by having a greater number of specific control objectives.
- Optimization: In the presence of multiple control objectives, it would be imperative to design an optimization technique to select the best possible control objective and the control parameters, based on given circumstances.
- Adaptive Control: An important addition to the control system is the property of adaptiveness. It is realized that, as the speed is changed there arises a need to change the control parameters as well. But, having an adaptive control system can make its direct implementation on real-world cars possible.
- Integrated Control: A lucrative area of work is the development of an integrated control system, comprising of one or more standard active safety systems and the active aerodynamic system. The most suitable of them is the integration of differential braking and active aerodynamic control. It is expected that the improvements in the performance of the vehicle will be substantial with such a type of control system.

References

[1] "The United Nations and Road Safety." [Online]. Available: https://www.un.org/en/roadsafety/report.shtml. [Accessed: 07-Apr-2019].

[2] T. Sikder, S. Kapoor, and Y. He, "Optimizing Dynamic Performance of High-Speed Road Vehicles Using Aerodynamic Aids," presented at the ASME 2016 International Mechanical Engineering Congress and Exposition, 2016, p. V007T09A060-V007T09A060.

[3] F. Diba, A. Barari, and E. Esmailzadeh, "Handling and safety enhancement of race cars using active aerodynamic systems," *Vehicle system dynamics*, vol. 52, no. 9, pp. 1171–1190, 2014.

[4] A. Hosseinian Ahangarnejad and S. Melzi, "Numerical analysis of the influence of an actively controlled spoiler on the handling of a sports car," *Journal of Vibration and Control*, vol. 24, no. 22, pp. 5437–5448, 2018.

[5] M. Abe, N. Ohkubo, and Y. Kano, "A direct yaw moment control for improving limit performance of vehicle handling-comparison and cooperation with 4WS," *Vehicle System Dynamics*, vol. 25, no. S1, pp. 3–23, 1996.

[6] M. Yamashita, K. Fujimori, K. Hayakawa, and H. Kimura, "Application of H∞ control to active suspension systems," *Automatica*, vol. 30, no. 11, pp. 1717–1729, 1994.

[7] Y. Shibahata, K. Shimada, and T. Tomari, "Improvement of vehicle maneuverability by direct yaw moment control," *Vehicle System Dynamics*, vol. 22, no. 5–6, pp. 465–481, 1993.

[8] M. Nagai, Y. Hirano, and S. Yamanaka, “Integrated control of active rear wheel steering and direct yaw moment control,” *Vehicle System Dynamics*, vol. 27, no. 5–6, pp. 357–370, 1997.

[9] A. HIGUCHI and Y. SAITOH, “Optimal control of four wheel steering vehicle,” *Vehicle System Dynamics*, vol. 22, no. 5–6, pp. 397–410, 1993.

[10] J. W.: MSFC, “What Is Aerodynamics?,” *NASA*, 12-May-2015. [Online]. Available: http://www.nasa.gov/audience/forstudents/k-4/stories/nasa-knows/what-is-aerodynamics-k4.html. [Accessed: 07-Apr-2019].

[11] R. H. Barnard, Road vehicle aerodynamic design-an introduction. 2001.

[12] J.-F. Beaudoin and J.-L. Aider, “Drag and lift reduction of a 3D bluff body using flaps,” *Experiments in fluids*, vol. 44, no. 4, p. 491, 2008.

[13] G. Fourrié, L. Keirsbulck, L. Labraga, and P. Gilliéron, “Bluff-body drag reduction using a deflector,” *Experiments in Fluids*, vol. 50, no. 2, pp. 385–395, 2011.

[14] X. Zhang, W. Toet, and J. Zerihan, “Ground effect aerodynamics of race cars,” *Applied Mechanics Reviews*, vol. 59, no. 1, pp. 33–49, 2006.

[15] C. Baker, F. Cheli, A. Orellano, N. Paradot, C. Proppe, and D. Rocchi, “Cross-wind effects on road and rail vehicles,” *Vehicle system dynamics*, vol. 47, no. 8, pp. 983–1022, 2009.

[16] J. Mohrfeld-Halterman and M. Uddin, “High fidelity quasi steady-state aerodynamic model effects on race vehicle performance predictions using multi-body simulation,” *Vehicle System Dynamics*, vol. 54, no. 7, pp. 963–981, 2016.

[17] J. A. Mohrfeld-Halterman and M. Uddin, “High fidelity quasi steady state aerodynamic model development and effects on race vehicle performance predictions,” *SAE International Journal of Passenger Cars-Mechanical Systems*, vol. 9, no. 2016-01–1589, pp. 603–611, 2016.

[18] J. Y. Wong, *Theory of ground vehicles*. John Wiley & Sons, 2008.

[19] S. Singh, L. Rai, P. Puri, and A. Bhatnagar, “Effect of moving surface on the aerodynamic drag of road vehicles,” *Proceedings of the Institution of Mechanical Engineers, Part D: Journal of Automobile Engineering*, vol. 219, no. 2, pp. 127–134, 2005.

[20] S.-O. Kang *et al.*, “Actively translating a rear diffuser device for the aerodynamic drag reduction of a passenger car,” *International Journal of Automotive Technology*, vol. 13, no. 4, pp. 583–592, 2012.

[21] A. R. Savkoor and C. Chou, “Application of aerodynamic actuators to improve vehicle handling,” *Vehicle System Dynamics*, vol. 32, no. 4–5, pp. 345–374, 1999.

[22] F. Diba, A. Barari, and E. Esmailzadeh, “Active Aerodynamic System to Improve the Safety and Handling of Race Cars in Lane Change and Wet Road Maneuvers,” presented at the ASME 2012 International Design Engineering Technical Conferences and Computers and Information in Engineering Conference, 2012, pp. 417–423.

[23] Y. He, “Design of an Actively Controlled Aerodynamic Wing to Increase High-Speed Vehicle Safety,” 2013.

[24] C. Doniselli, G. Mastinu, and M. Gobbi, “Aerodynamic effects on ride comfort and road holding of automobiles,” *Vehicle System Dynamics*, vol. 25, no. S1, pp. 99–125, 1996.

[25] A. Savkoor, S. Manders, and P. Riva, “Design of actively controlled aerodynamic devices for reducing pitch and heave of truck cabins,” *JSAE review*, vol. 22, no. 4, pp. 421–434, 2001.

[26] J. Meijaard, A. Savkoor, and G. Lodewijks, “Potential for vehicle ride improvement using both suspension and aerodynamic actuators,” presented at the Proceedings of

the IEEE International Symposium on Industrial Electronics, 2005. ISIE 2005., 2005, vol. 1, pp. 385–390.

[27] M. Corno, S. Bottelli, G. Panzani, M. Tanelli, C. Spelta, and S. Savaresi, "Improving high speed road-holding using actively controlled aerodynamic surfaces," presented at the 2013 European Control Conference (ECC), 2013, pp. 1493–1498.

[28] M. Corno, S. Bottelli, M. Tanelli, C. Spelta, and S. M. Savaresi, "Active control of aerodynamic surfaces for ride control in sport vehicles," *IFAC Proceedings Volumes*, vol. 47, no. 3, pp. 7553–7558, 2014.

[29] D. T. Ayyagari and Y. He, "Aerodynamic analysis of an active rear split spoiler for improving lateral stability of high-speed vehicles," *International Journal of Vehicle Systems Modelling and Testing*, vol. 12, no. 3–4, pp. 217–239, 2017.

[30] M. Hammad, K. Qureshi, and Y. He, "Safety and Lateral Dynamics Improvement of a Race Car Using Active Rear Wing Control," SAE Technical Paper, 0148–7191, 2019.

[31] "ISO 8855:2011(en), Road vehicles — Vehicle dynamics and road-holding ability — Vocabulary.".

[32] "Is it possible to change the orientation of the default geometry?," *Onshape*. [Online]. Available: https://forum.onshape.com/discussion/6555/is-it-possible-to-change-the-orientation-of-the-default-geometry. [Accessed: 01-Jul-2019].

[33] W. F. Milliken and D. L. Milliken, *Race car vehicle dynamics*, vol. 400. Society of Automotive Engineers Warrendale, 1995.

[34] T. D. Gillespie, "Fundamentals of vehicle dynamics," SAE Technical Paper, 1992.

[35] K. Ogata, *Modern Control Engineering*, 5 edition. Pearson, 2011.

[36] H. K. Khalil and J. W. Grizzle, *Nonlinear systems*, vol. 3. Prentice hall Upper Saddle River, NJ, 2002.

[37] J. Liu and X. Wang, Advanced sliding mode control for mechanical systems. Springer, 2012.

[38] N. Matsumoto and M. Tomizuka, "Vehicle lateral velocity and yaw rate control with two independent control inputs," presented at the 1990 American Control Conference, 1990, pp. 1868–1875.

[39] S. Zhu and Y. He, "A driver-adaptive stability control strategy for sport utility vehicles," *Vehicle system dynamics*, vol. 55, no. 8, pp. 1206–1240, 2017.

[40] H. Pacejka, *Tire and vehicle dynamics*. Elsevier, 2005.

[41] "CarSim Overview." [Online]. Available: https://www.carsim.com/products/carsim/index.php. [Accessed: 26-Jun-2019].

[42] "S1223 (s1223-il)." [Online]. Available: http://airfoiltools.com/airfoil/details?airfoil=s1223-il. [Accessed: 18-Apr-2019].

[43] *Separation of Flow*. Elsevier, 1970.

Appendix

Parameters	Values	Parameters	Values
a	0.4 m	l_1	1.402 m
b	2 m	l_2	1.646 m
C	11000 N/mm-s	l	3.048 m
C_y	65000 N/rad	m_{us}	90 kg
E	0.5	m_s	1653 kg
g	9.81 m/s^2	m	1833 kg
h	0.59 m	R_s	17.25
h_{roll}	0.56 m	R_{rp}	0.1 mm/deg
h_f	0.35 m	R_{lsr}	0.495 deg/mm
h_r	0.35 m	R_{rsr}	0.607 deg/mm
h_{12}	0.2 m	T	1.6 m
h_{34}	0.3 m	u	80-200 km/hr
I_{xx}	614 kg-m^2	U	0.5-1.5
I_{zz}	2765 kg-m^2	μ	0.5 or 0.85
K_f	34000 N/mm	ρ	1.225 kg/m^3
K_r	46000 N/mm		